

<i>Title:</i> NEON Imaging Spectrometer Geolocation Algorithm Theoretical Basis Document		<i>Date:</i> 11/20/2015
<i>NEON Doc. #:</i> NEON.DOC.001290	<i>Author:</i> T. Kampe, W. Gallery	<i>Revision:</i> B

NEON IMAGING SPECTROMETER GEOLOCATION PROCESSING ALGORITHM THEORETICAL BASIS DOCUMENT

PREPARED BY	ORGANIZATION	DATE
Thomas Kampe, William Gallery	AOP	01/07/2013

APPROVALS	ORGANIZATION	APPROVAL DATE
Hanne Buur	PSE	11/06/2015
Dave Tazik	SCI	10/14/2015
Andrea Thorp	SCI	10/23/2015
Shelley Petroy	DPS	11/06/2015

RELEASED BY	ORGANIZATION	RELEASE DATE
Judy Salazar	CM	11/20/2015

See configuration management system for approval history.

© 2015 NEON Inc. All rights reserved.

<i>Title:</i> NEON Imaging Spectrometer Geolocation Algorithm Theoretical Basis Document		<i>Date:</i> 11/20/2015
<i>NEON Doc. #:</i> NEON.DOC.001290	<i>Author:</i> T. Kampe, W. Gallery	<i>Revision:</i> B

Change Record

REVISION	DATE	ECO #	DESCRIPTION OF CHANGE
A	08/25/2014	ECO-01765	Initial release
B	11/20/2015	ECO-02315	Major revision; added Appendix C

Title: NEON Imaging Spectrometer Geolocation Algorithm Theoretical Basis Document		Date: 11/20/2015
NEON Doc. #: NEON.DOC.001290	Author: T. Kampe, W. Gallery	Revision: B

TABLE OF CONTENTS

1	DESCRIPTION	1
1.1	Purpose	1
1.2	Scope.....	1
2	RELATED DOCUMENTS AND ACRONYMS.....	1
2.1	Applicable Documents	1
2.2	Reference Documents.....	2
2.3	External References	2
2.4	Acronyms	2
3	DATA PRODUCT DESCRIPTION	3
3.1	Variables Reported	3
3.2	Input Dependencies	4
3.3	Product Instances.....	7
3.4	Temporal Resolution and Extent	7
3.5	Spatial Resolution and Extent	7
4	SCIENTIFIC CONTEXT	7
4.1	Theory of Measurement/Observation.....	8
4.2	Theory of Algorithm	11
5	ALGORITHM IMPLEMENTATION	15
5.1	Production Processing Flow	15
6	UNCERTAINTY.....	18
6.1	Analysis of Uncertainty	18
6.2	Reported Uncertainty	19
7	VALIDATION AND VERIFICATION	20
7.1	Algorithm Validation	20
7.2	Data Product Validation.....	21
8	SCIENTIFIC AND EDUCATIONAL APPLICATIONS	21
9	FUTURE MODIFICATIONS AND PLANS.....	21
10	BIBLIOGRAPHY	22
	APPENDIX A SCANNING GEOMETRIES OF THE NEON REMOTE SENSING INSTRUMENTS.....	23
	APPENDIX B LIST OF FILES.....	31
	APPENDIX C MATHEMATICS OF GEOLOCATION.....	32

Title: NEON Imaging Spectrometer Geolocation Algorithm Theoretical Basis Document		Date: 11/20/2015
NEON Doc. #: NEON.DOC.001290	Author: T. Kampe, W. Gallery	Revision: B

LIST OF TABLES AND FIGURES

Table 1. Sample Step 1b Report File.....	16
Table 2. Co-registration error budget.....	20
Table 3. Imaging spectrometer geolocation error.....	20
Table 4. AOP Waveform Altimeter LiDAR requirements compared to the Optech ALTM Gemini Specification.....	25
Table 5. Applanix DSS 449 camera specifications.....	28
Table 6. Typical camera data acquisition parameters.....	29
Table 7. List of input, intermediate and output files.....	31
Table C-1 Variables reported in the sbet file.....	37
Figure 1. Sample GLT Image.....	4
Figure 2. NIS geolocation processing flow.....	6
Figure 3. Sample raw imaging spectrometer radiance image.....	9
Figure 4. Sample Orthorectified NEON Imaging Spectrometer Radiance Image.....	9
Figure 5. Euler Angles.....	11
Figure 6. Coordinate transformation from sensor frame to surface frame.....	12
Figure 7. NEON Remote Sensing Payload integrated into Twin Otter aircraft.....	13
Figure 8. Pushbroom imaging spectrometer concept.....	23
Figure 9. NIS flight geometry.....	24
Figure 10. WALi scan geometry.....	27
Figure 11. AOP camera scanning approach.....	29
Figure C-1. A right-handed Cartesian coordinate system.....	32
Figure C-2. Relationship between the b-frame and the s-frame.....	33
Figure C-3. The three Euler angle (ϕ , θ , φ) rotations about the z-axis (yaw), y-axis (pitch) and x-axis (roll.).....	34
Figure C-4. Sketch showing the m-frame, b-frame and s-frame.....	36
Figure C-5. Sketch showing the b-frame, the s-frame and the lever arm \mathbf{r}_s^b between the IMU and the sensor focal plane.....	37
Figure C-6. Sketch showing the LOS of a detector pixel for both the spectrometer and the digital camera.....	39
Figure C-7. Sketch of the image observation.....	41
Figure C-8. The location of the point P relative to the m-frame, the b-frame and the s-frame.....	42
Figure C-9. Sketch showing the LOS from the point P through the focal point f to where it intersects the camera sensor frame at pixel i,j	43

Title: NEON Imaging Spectrometer Geolocation Algorithm Theoretical Basis Document		Date: 11/20/2015
NEON Doc. #: NEON.DOC.001290	Author: T. Kampe, W. Gallery	Revision: B

1 DESCRIPTION

1.1 Purpose

This document details the algorithm used to orthorectify the raw data acquired by the NEON Imaging Spectrometer (NIS). The orthorectification of the NIS data is one of the critical processing steps in deriving the NEON Level-1 data product NEON.DOM.SIT.DP1.30008 Spectrometer Orthorectified at-Sensor Radiance from Level 0 data. The algorithm describes the production orthorectification process for NIS data, the calculation of observation geometry parameters, producing a mosaic of all flight lines collected over a site. The NEON.DOM.SIT.DP1.30008 data product is an intermediate data product in the production of the NEON.DOM.SIT.DP1.30006 L-1 Spectrometer Orthorectified Surface Directional Reflectance data product as described in RD[05]. This document includes a detailed discussion of measurement theory and implementation, appropriate theoretical background, data product provenance, quality assurance and control methods used, approximations and/or assumptions made, and a detailed exposition of uncertainty resulting in a cumulative reported uncertainty for this product.

1.2 Scope

This document describes the theoretical background and algorithmic process for orthorectification of the raw L-0 NEON imaging spectrometer data and co-location with simultaneously acquired LiDAR L-0 data as a necessary step to creating the NEON Level-1 data product NEON.DOM.SIT.DP1.30008 Spectrometer Orthorectified at-Sensor Radiance. It does not provide computational implementation details, except for cases where these stem directly from algorithmic choices explained here.

2 RELATED DOCUMENTS AND ACRONYMS

2.1 Applicable Documents

Applicable documents contain information that shall be applied in the current document. Examples are higher level requirements documents, standards, rules and regulations.

AD[01]	NEON.DOC.000001	NEON Observatory Design
AD[02]	NEON.DOC.005003	NEON Scientific Data Products Catalog
AD[03]	NEON.DOC.005004	NEON Level 1-3 Data Products Catalog
AD[04]	NEON.DOC.005005	NEON Level 0 Data Product Catalog
AD[05]	NEON.DOC.015005	AOP Technical and Operating Requirements
AD[06]	NEON.DOC.015015	AOP Platform Integration Mount Assembly
AD[07]	NEON.DOC.015018	ICD between AOP Payload and Aircraft
AD[08]	NEON.DOC.001292	NEON L0 to L1 Discrete Return Lidar ATBD
AD[09]	NEON.DOC.001211	NEON Digital Camera Orthorectification ATBD
AD[10]	NEON.DOC.000855	AOP Gemini LiDAR System Unit No. 1 Delivery Performance Report

Title: NEON Imaging Spectrometer Geolocation Algorithm Theoretical Basis Document		Date: 11/20/2015
NEON Doc. #: NEON.DOC.001290	Author: T. Kampe, W. Gallery	Revision: B

2.2 Reference Documents

Reference documents contain information complementing, explaining, detailing, or otherwise supporting the information included in the current document.

RD[01]	NEON.DOC.000008	NEON Acronym List
RD[02]	NEON.DOC.000243	NEON Glossary of Terms
RD[03]	NEON.DOC.001210	NEON Imaging Spectrometer Calibrated Radiance ATBD
RD[04]	NEON.DOC.001288	NEON Imaging Spectrometer L-1 Radiance to L-1 Reflectance ATBD
RD[05]	NEON.DOC.001289	NEON Imaging Spectrometer Level-1 Processing Overview Document
RD[06]	NEON.DOC.001277	AOP Directory and File Name Conventions

2.3 External References

External references contain information pertinent to this document, but are not NEON configuration-controlled. Examples include manuals, brochures, technical notes, and external websites.

ER [01]	
ER [02]	
ER [03]	

2.4 Acronyms

Acronym	Explanation
ATBD	Algorithm Theoretical Basis Document
IGM	Input Geometry Matrix
GLT	Geometric Lookup Table
ORT	Ortho <u>r</u> Rectified <u>i</u> magery Table
OBS	Observation geometry parameter file in pixel-by-pixel format
DP	Data Product
L0	Level 0
L1	Level 1
UQ	Unquantifiable Uncertainty

Title: NEON Imaging Spectrometer Geolocation Algorithm Theoretical Basis Document		Date: 11/20/2015
NEON Doc. #: NEON.DOC.001290	Author: T. Kampe, W. Gallery	Revision: B

3 DATA PRODUCT DESCRIPTION

3.1 Variables Reported

The primary outputs from the NEON Imaging Spectrometer (NIS) geolocation algorithm are listed below. Two intermediate data files that are retained for later processing steps are the Input Geometry Files and the Ortho-rectified Geometric Lookup Table file as described in NEON.DOC.001277 AOP Directory and File Name Conventions (RD[06]). These are:

- Input Geometry File:** Input geometry files (named with “_igm” file extensions) denote the UTM Easting and Northing values derived by the geocorrection process for each original image pixel. If a nominal NIS scene is 598 samples, 1000 lines and 428 bands, then its corresponding input geometry file will be 598 samples, 1000 lines and 2 bands. The first band contains UTM Easting values in meters and the second band contains UTM Northing values in meters for each original pixel. The input geometry files have the same spatial size as the raw NIS imagery. The file is double precision, binary data in a Band Interleaved by Line (BIL) format. The scene elevation, pixel size and UTM zone number information are given in an associated ASCII header file. The input geometry file itself is not orthorectified, but does contain the geolocation information for each original raw pixel.
- Ortho-corrected geometric lookup table (GLT) files:** Ortho-corrected geometric lookup table files (named with “_glt” file extensions) that contain much of the important information that is created in the geocorrection process. The “_glt” file contains information about which original pixel occupies which output pixel in the final product. Additionally, it is sign-coded to indicate if a certain output pixel is “real” or a nearest-neighbor infill pixel. The “_glt” file is an [orthorectified product](#), with a fixed pixel size projected into a rotated UTM system. The pixel size, scene elevation, UTM zone number and rotation angle information is reported in an associated ASCII header file. The “_glt” file itself is two-byte integer binary data in a BIL format. The two bands of the “_glt” file refer to original sample number and original line number; respectively. The sign of the value indicates whether the pixel is an actual image pixel, located at its proper position (indicated by a positive value) or a nearest-neighbor infill pixel placed to fill an undersampling image gap (indicated by a negative value). The geometric lookup table image, along with the raw imagery, can be used to geocorrect any band or derived product through a simple lookup table procedure. A sample GLT image is shown in Figure 1.

Two data files are produced as the final output of the geolocation processing. The first of these are used to produce the L-1 Ortho-rectified spectral radiance data Product.

- OrthoRectified imagery Table (ORT) files:** Orthorectified imagery Table files are produced by applying the geometric lookup tables to the entire NIS data set (i.e., all spectral bands) to create a fully orthorectified image cube. These files (named with “__geo” extensions) represent the final imaging spectrometer orthorectified radiances at the flight line level.

Title: NEON Imaging Spectrometer Geolocation Algorithm Theoretical Basis Document		Date: 11/20/2015
NEON Doc. #: NEON.DOC.001290	Author: T. Kampe, W. Gallery	Revision: B

- **Mosaic multi-file mosaic (MOS_ORT) orthorectified files:** the MOS_ORT files are mosaics of multiple flight lines of the orthorectified radiances stored as a single file.

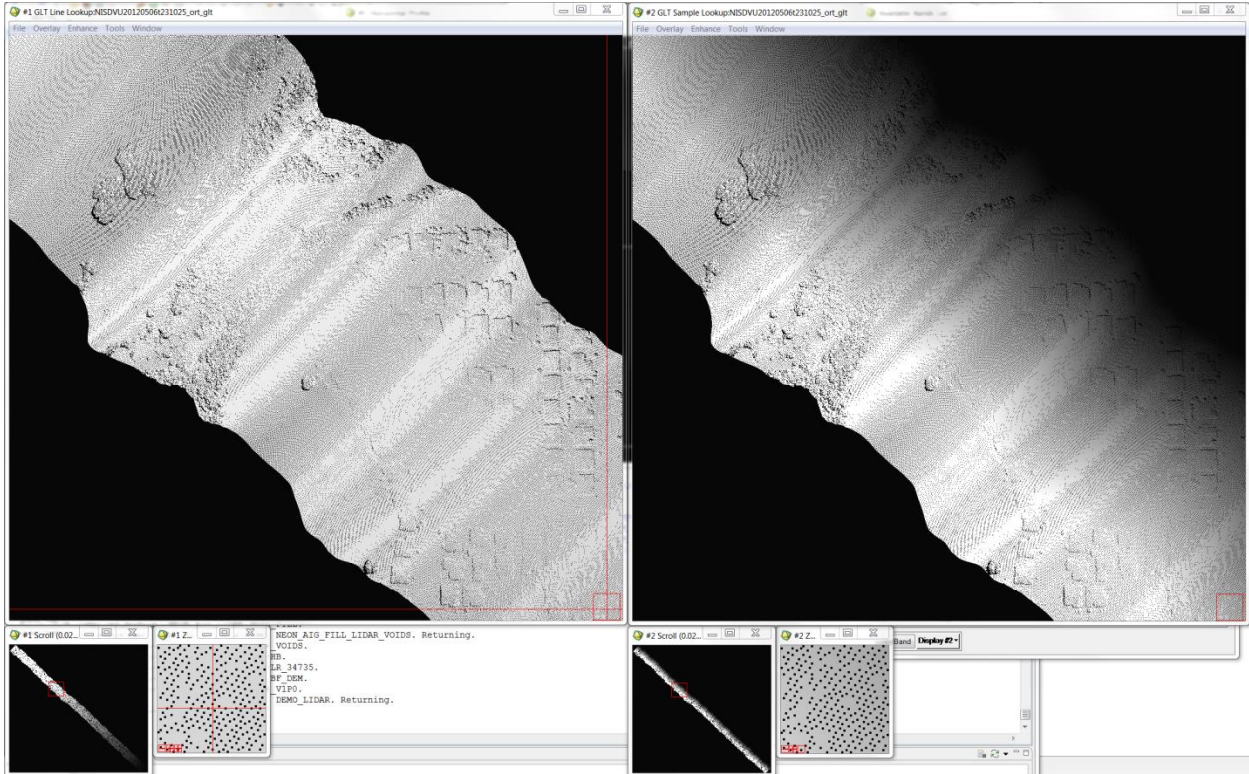


Figure 1. Sample GLT Image. The GLT files contain information about which original pixel occupies which output pixel in the final product. The GLT output is sign-coded to indicate whether a certain pixel contains real data (positive) or if it is nearest-neighbor infill pixel (negative).

3.2 Input Dependencies

There are several necessary inputs required to support the geolocation processing of the NEON imaging spectrometer data. These are provided from the LiDAR processing and external data sources. These inputs are described in the following paragraphs and represented in the processing flow diagram in Figure 2.

- **Earth Gravitational Model 1996 (EGM96) EGM96 Geoid file:** An individual file is created for each region flown. An improved spherical harmonic model of the Earth's gravitational potential to degree 360 developed by the NASA Goddard Space Flight Center (GSFC), the National Imagery and Mapping Agency (NIMA), and the Ohio State University (OSU). The new model, Earth Gravitational Model 1996 incorporates improved surface gravity data, altimeter-derived anomalies from ERS-1 and from the GEOSAT Geodetic Mission (GM), extensive satellite tracking

Title: NEON Imaging Spectrometer Geolocation Algorithm Theoretical Basis Document		Date: 11/20/2015
NEON Doc. #: NEON.DOC.001290	Author: T. Kampe, W. Gallery	Revision: B

data - including new data from Satellite laser ranging (SLR), the Global Positioning System (GPS), NASA's Tracking and Data Relay Satellite System (TDRSS), the French DORIS system, and the US Navy TRANET Doppler tracking system - as well as direct altimeter ranges from TOPEX/POSEIDON (T/P), ERS-1, and GEOSAT. The final solution blends a low-degree combination model to degree 70, a block-diagonal solution from degree 71 to 359, and a quadrature solution at degree 360. The model was used to compute geoid undulations accurate to better than one meter (with the exception of areas void of dense and accurate surface gravity data) and provide WGS84 as a true three-dimensional reference system (<http://cddis.nasa.gov/926/egm96/nasatm.html>).

- **SBET (smoothed best estimate trajectory) file:** this file is a product of the LiDAR geolocation processing.
- **Processed radiance file:** this is the spectrometer spectral radiance data, as processed through the NIS calibration algorithm (RD [03]).
- **Merged Digital Elevation Map (DEM) for region of interest:** a DEM is generated during the LiDAR geolocation processing but this may have gaps in coverage (between flight lines, etc.). For this reason the LiDAR-generated DEM is merged with an externally-generated DEM (typically, a USGS product) to create the merged DEM providing full spatial coverage of the region of interest. The merged DEM is a product of the LiDAR processing.
- **NIS Camera Model:** this model provides as input the distortion introduced by the imaging spectrometer into the retrieved data and the measured lever arms between the NIS focal plane and the LiDAR scan mirror. These parameters are unique to each NIS instrument and in the case of the lever arms, unique to each installation of the NIS into the aircraft. The NIS distortion, characterized by the measured curvature of the projected focal plane, is provided as part of the instrument calibration file by the instrument vendor, NASA JPL. This information is coded into the unique camera file for each instrument one time. As stated previously, the NIS focal plane-to-LiDAR mirror lever arms must be measured for each installation in to the aircraft and are manually entered in the `neon_aig_vswir_ortho_apply_lever_arm.pro` subroutine prior to processing.

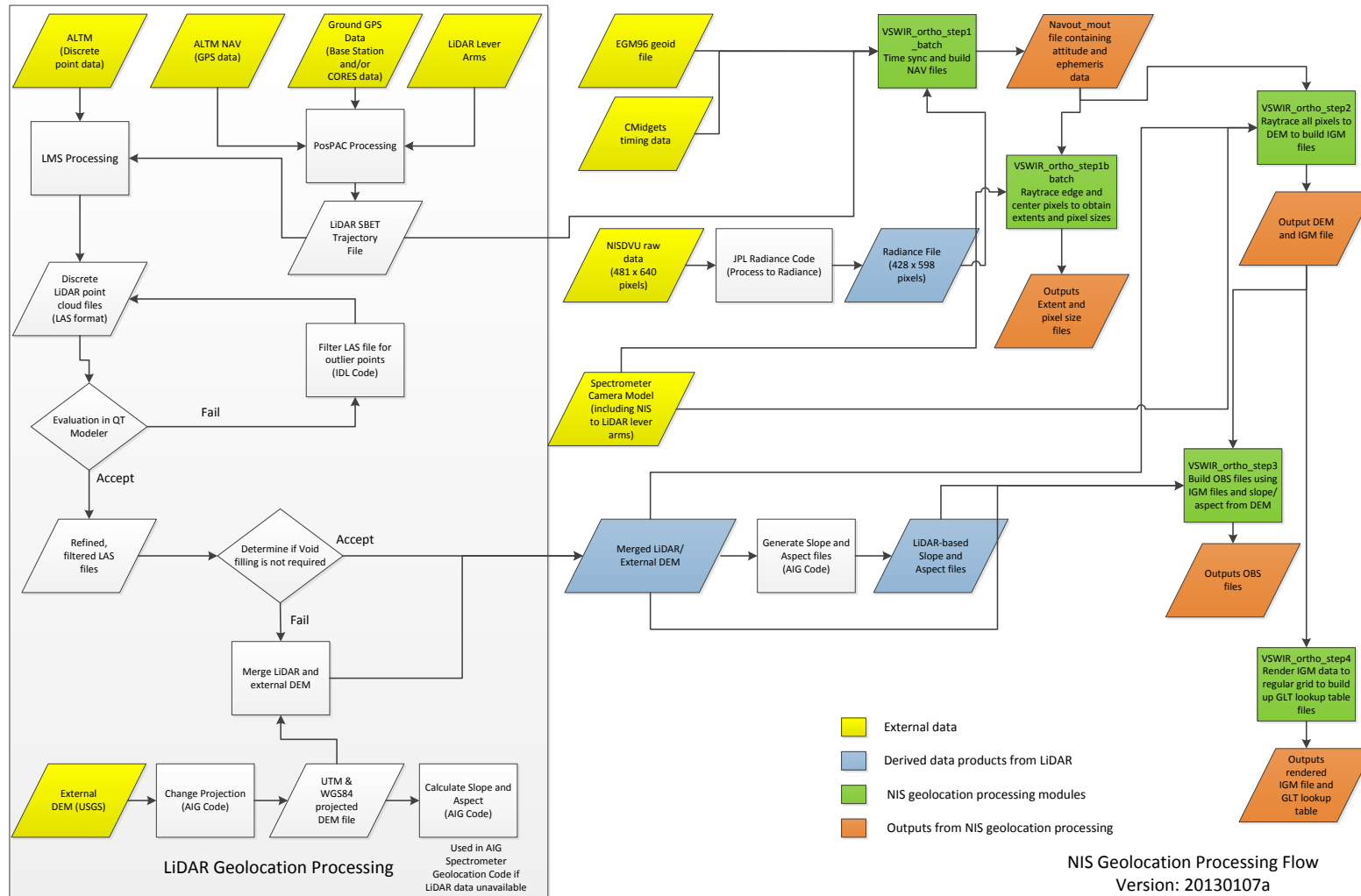


Figure 2. NIS geolocation processing flow

<i>Title:</i> NEON Imaging Spectrometer Geolocation Algorithm Theoretical Basis Document		<i>Date:</i> 11/20/2015
<i>NEON Doc. #:</i> NEON.DOC.001290	<i>Author:</i> T. Kampe, W. Gallery	<i>Revision:</i> B

3.3 Product Instances

The NEON.DOM.SIT.DP1.30008 L-1 Spectrometer Orthorectified at-Sensor Radiance L-1 Data Product is a product of this algorithm.

3.4 Temporal Resolution and Extent

The NIS geolocation algorithm is applied on each AOP flight line, which typically measure between 5 and 20 km in length and approximately 600 m in width. Typical flight altitudes are approximately 1000m Above Ground Level (AGL). Flight speeds are generally around 100 knots (185.2 km/hour), and therefore, the time required to acquire flight lines of the lengths stated will range from 1.6 to 6.5 minutes. The integration time for the NIS detector array is 100 milliseconds, so an image is acquired every 100 milliseconds along-track.

3.5 Spatial Resolution and Extent

The NIS geolocation algorithm is applied on each AOP flight line, which typically measure between 5 and 20 km in length and approximately 600 m in width. The Instantaneous Field of View (IFOV) of the NEON Imaging Spectrometer is 1.0 milliradian, which equates to a ground sampling distance (GSD) of 1 meter at a nominal flight of 1000 m above ground. The actual ground resolution will vary with flight altitude and cross-track field angle.

4 SCIENTIFIC CONTEXT

A critical first step in the processing of imaging spectrometer data is the accurate orthorectification of the raw data to eliminate the distortion introduced by aircraft motion and atmospheric turbulence. In addition, in this process the spectrometer data is co-registered to the LiDAR data that is acquired simultaneously from the NEON Airborne Observation Platform (AOP). The outputs from this processing are accurate projections of each individual imaging spectrometer pixel onto a map grid and the precise geometric coordinates for each pixel. The high precision and high accuracy trajectory and attitude information obtained from the onboard GPS/INS system form the common link for the detailed ray tracing of the NEON imaging spectrometer, LiDAR, and subsequently, the digital camera. These sensors all receive the same GPS time stamping from the imaging spectrometer IMU, which allows for the common use of the GPS-IMU data between instruments. The LiDAR GPS and Inertial Measurement Unit (IMU) accelerometers provide the precise information on aircraft position and attitude; respectively. Measurements of the lever-arms (or offsets) between the GPS antenna, IMU, LiDAR, and imaging spectrometer optical centers and subsequent optimization in the optical models of the two sensor heads provide the precise co-location and projected geo-location of all data in post-flight processing.

<i>Title:</i> NEON Imaging Spectrometer Geolocation Algorithm Theoretical Basis Document		<i>Date:</i> 11/20/2015
<i>NEON Doc. #:</i> NEON.DOC.001290	<i>Author:</i> T. Kampe, W. Gallery	<i>Revision:</i> B

4.1 Theory of Measurement/Observation

The remote sensing payload being flown onboard NEON’s Airborne Observation Platform (AOP) includes the NEON Imaging Spectrometer (NIS), a visible-to-shortwave infrared (VSWIR) pushbroom imaging spectrometer (NIS); a small-footprint full waveform LiDAR, and a high-resolution digital camera (AD[05]). The instrument payload is mounted onto a common integration plate, the Platform Integration Mount, or PIM (AD[06]). The entire AOP remote sensing payload is integrated onto a de Havilland DHC-6 Twin Otter aircraft configured with a large open downward-looking viewing port. The payload is mounted directly on the cabin floor via the seat rails with the sensors viewing in the nadir direction through the open port (AD[07]).

Since the payload is mounted directly to the airframe, there is no active roll compensation during flight. Any aircraft motion or vibration will result in image distortion. The raw imagery acquired with the NIS and LiDAR is usually distorted by turbulence and aircraft roll, pitch, and yaw (Figure 3). Following the orthorectification and co-location process described in this document, ortho-rectification of the spectrometer data is achieved referenced to a uniform grid defined by the LiDAR data as shown in Figure 4. Through this process, the imaging spectrometer data is also co-registered to data retrieved by the LiDAR. Co-registration between the two instruments is particularly challenging due to the different scanning geometries employed by the two sensors (Appendix 1. Scanning Geometries of the LiDAR and NIS).

For this reason, a necessary first step in the L-0 to L-1 imaging spectrometer data processing chain is the precision orthorectification of the LiDAR discrete return ranges. This aspect of the processing chain is described in the NEON L0 to L1 Discrete Return LiDAR Algorithm Theoretical Basis Document (AD[08]).

The Optech Gemini LiDAR is provided with a high accuracy Applanix Inertial Measurement Unit (IMU) and GPS system. The positional information from the GPS and the 3-axis attitude data from the IMU accelerometers are combined in a tightly coupled Kalman filter approach to give real-time information on the x, y, and z position as well as roll, pitch, and true heading of the sensors on board the aircraft. The IMU that is installed on the platform integration mount as part of the NIS system is used exclusively to provide a timestamp for acquired data frames from the imaging spectrometer.

Title: NEON Imaging Spectrometer Geolocation Algorithm Theoretical Basis Document		Date: 11/20/2015
NEON Doc. #: NEON.DOC.001290	Author: T. Kampe, W. Gallery	Revision: B



Figure 3. Sample raw imaging spectrometer radiance image

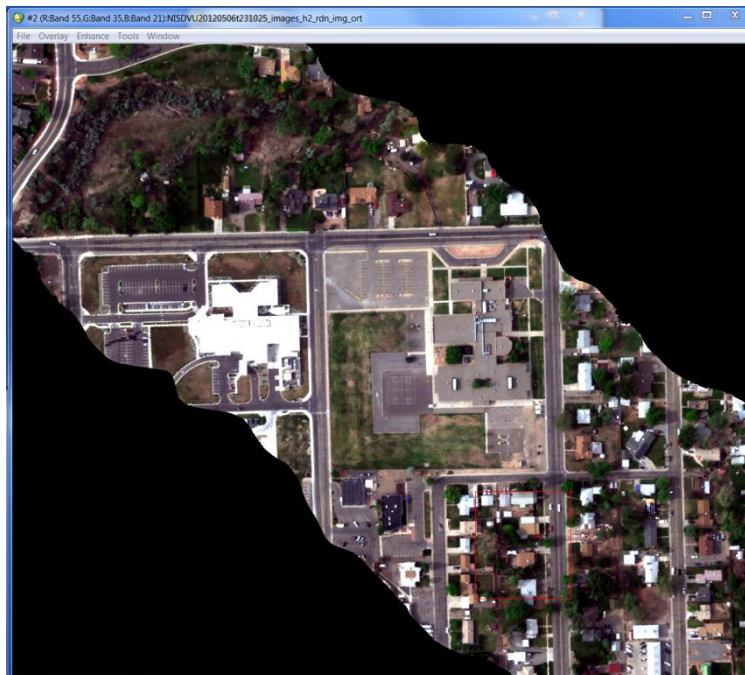


Figure 4. Sample Orthorectified NEON Imaging Spectrometer Radiance Image

<i>Title:</i> NEON Imaging Spectrometer Geolocation Algorithm Theoretical Basis Document		<i>Date:</i> 11/20/2015
<i>NEON Doc. #:</i> NEON.DOC.001290	<i>Author:</i> T. Kampe, W. Gallery	<i>Revision:</i> B

In the imaging spectrometer geolocation procedure, each pixel is individually raytraced from the airborne platform to the ground using a full optical sensor model and trajectory data. The geolocation of the LiDAR data is conducted prior to processing of the imaging spectrometer data and a digital elevation map (DEM) is generated from the LiDAR first returns. This process is described in AD[07]. The pixels at the focal plane of the imaging spectrometer are then ray traced to the surface defined by the DEM generated from the DEM data.

The general method employed in the orthorectification of the imaging spectrometer data and co-registration to the LiDAR data is the use of the standard Euler Angle (Figure 5) approach to rotate the NIS principal plane according to the roll, pitch, and true heading of the aircraft that is recorded by the Applanix IMU integral to the LiDAR system. By accounting for aircraft velocity, the timing of focal plane image acquisition, lever arms between the LiDAR and imaging spectrometer, and incorporating an accurate camera model for the spectrometer, a position and pointing vector is calculated for each NIS image pixel. Best estimates of each imaging spectrometer pixel location center with respect to the geodesic coordinates defined by the LiDAR DEM in three dimensions are made to produce co-located and orthorectified maps of the imaging spectrometer and LiDAR data that are reported on the Universal Transverse Mercator (UTM) projection system. The precision locational information for each imaging spectrometer pixel is then available for detailed spectroscopic modeling and is used in subsequent processing for rendering the LiDAR and imaging spectrometer data sets onto a common grid for overlay, comparison, and product generation. A similar processing methodology is employed to orthorectify the digital camera imagery to the common grid defined by the LiDAR -generated DEM (AD[09]).

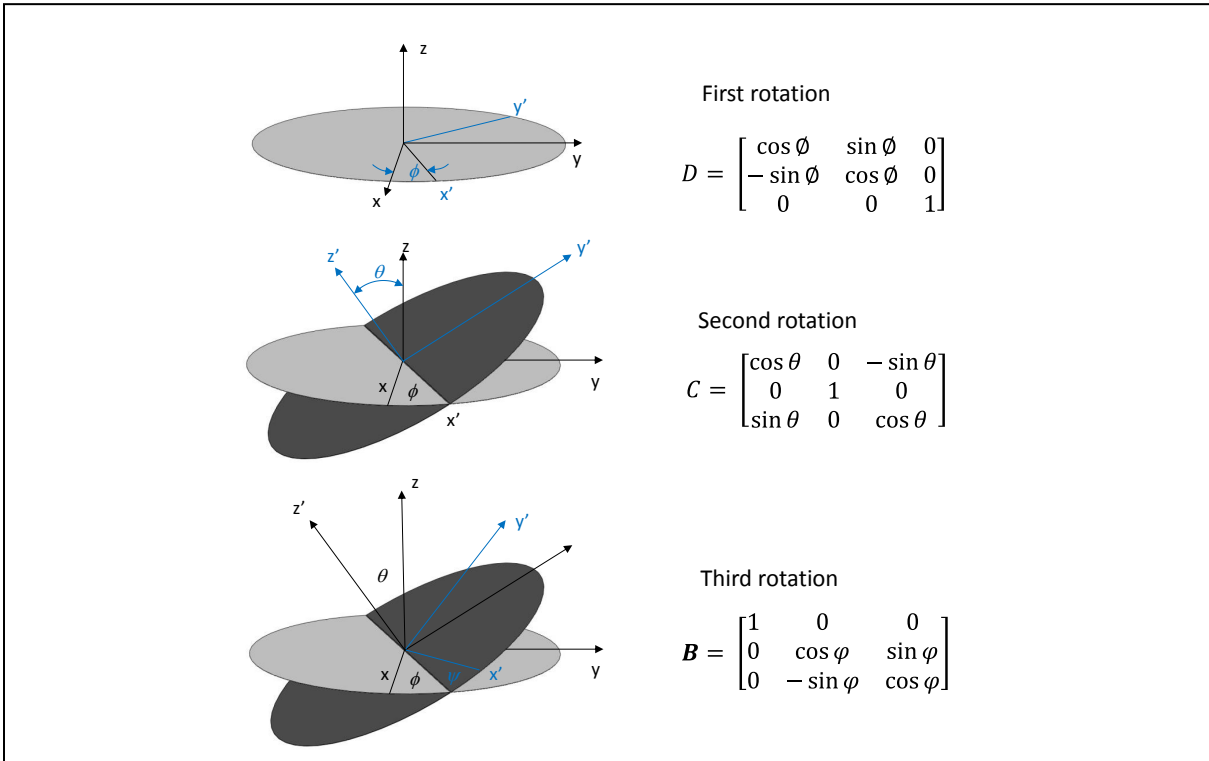


Figure 5. Euler Angles

4.2 Theory of Algorithm

The georeferencing of the airborne imaging spectrometer data is a problem of transforming the 3-D coordinate vector r^s of the spectrometer sensor frame (s-frame) to the 3-D coordinate vector r^m of the mapping frame on the earth surface. The method described here follows the method described in *El-Sheimy, (2009)*. The transformation between the spectrometer sensor reference frame (s-frame) and the mapping frame of the earth surface (m-frame) is illustrated in Figure 6.

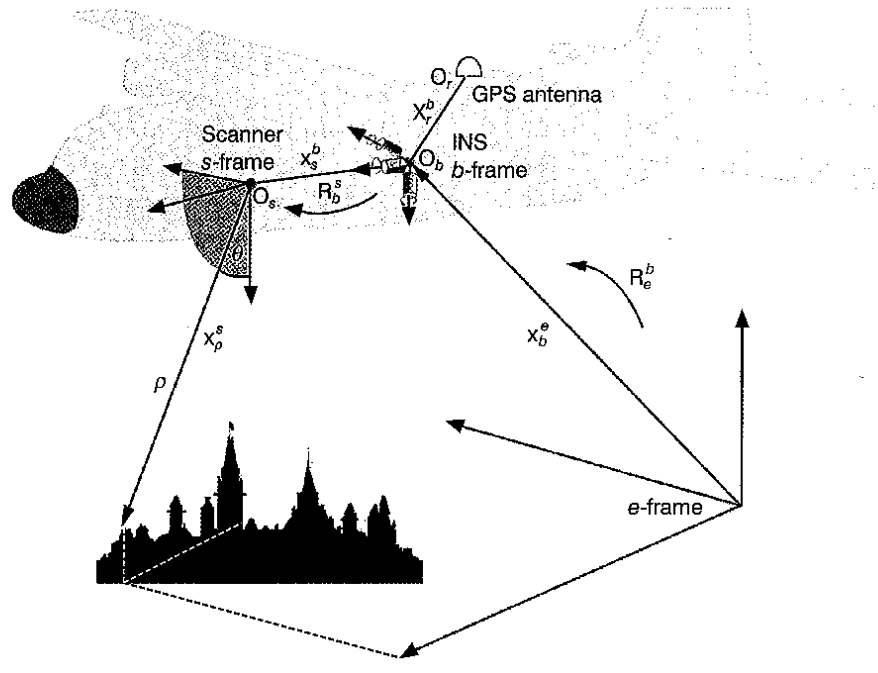


Figure 6. Coordinate transformation from sensor frame to surface frame

The sensor reference frame (S-frame) changes position and orientation with respect to the mapping reference frame (m-frame) with time as a result of aircraft velocity, elevation, and orientation. Georeferencing is possible at any instant of time (t), if the sensor position in the m-frame (r_i^m) and the rotation matrix between the S-frame and the m-frame, $R_s^m(t)$, is known. The georeferencing equation can then be written for any object point (i) as

$$r_i^m = r_s^m(t) + R_s^m(t)r_i^s \tag{1}$$

where

r_i^m is the position vector of an object in the m-frame;

(t) is the instant of time;

And, r_i^s is the position vector of an object (i) in the S-frame which is given by

$$r_i^s = \begin{bmatrix} -d \sin \alpha \\ 0 \\ -d \cos \alpha \end{bmatrix} \tag{2}$$

However, Equation 1 is only a first approximation of the actual situation. It implies that the location of the center of the sensor can be directly determined from this equation. This is ~~the~~ however not the case for the AOP payload since the navigation sensors – the GPS antenna and IMU – are not in the same location in space as the NIS sensor. Thus, it is necessary to account for the translations and rotations between these different instruments. The relative positions of the instruments on the platform

Title: NEON Imaging Spectrometer Geolocation Algorithm Theoretical Basis Document		Date: 11/20/2015
NEON Doc. #: NEON.DOC.001290	Author: T. Kampe, W. Gallery	Revision: B

integration mount are shown in Figure 7. The measured offsets between these instruments are referred to as *lever arms*. As an example, the lever arms for the NEON Imaging Spectrometer Design Verification Unit in the configuration flown during 2012 are shown in Figure 8.

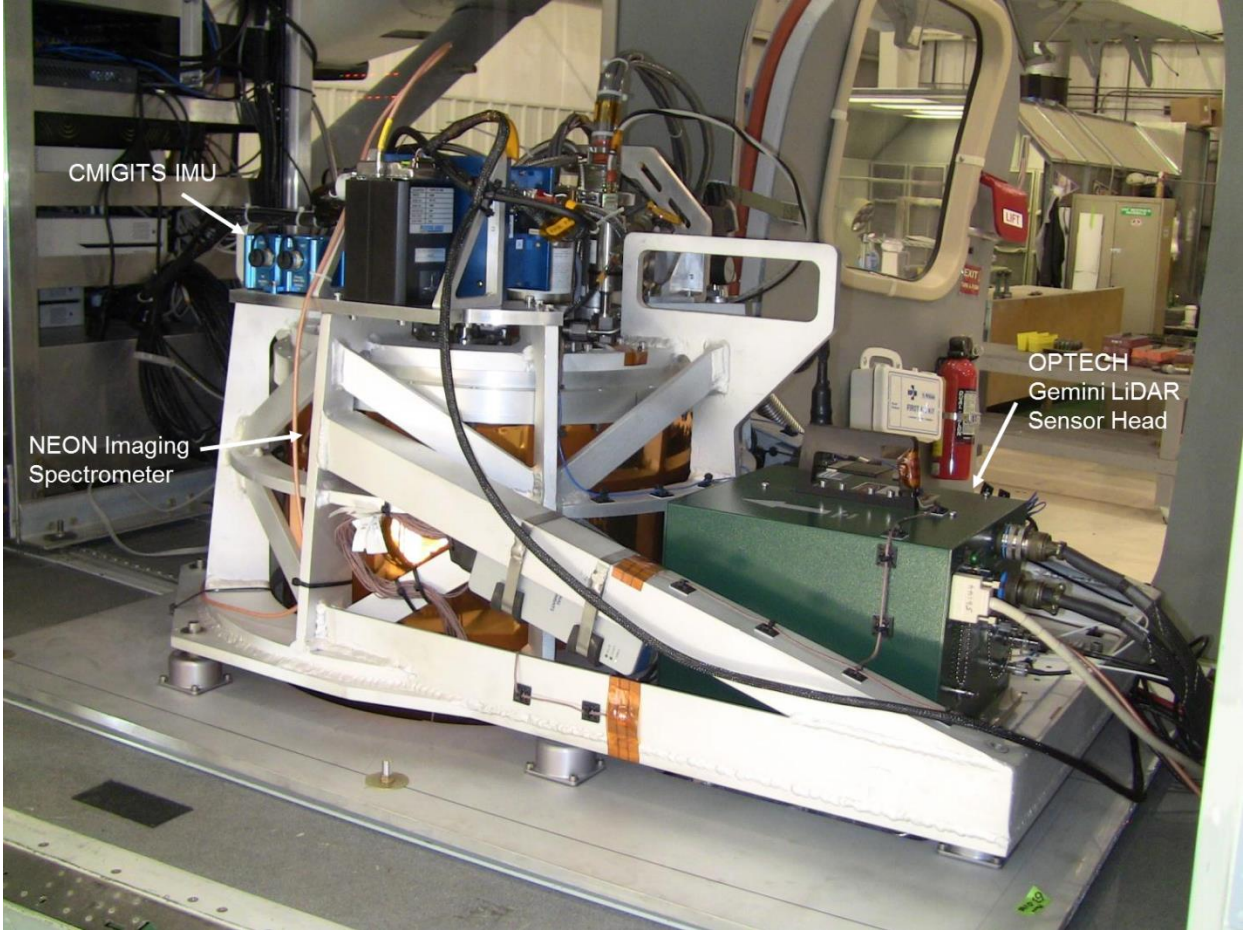


Figure 7. NEON Remote Sensing Payload integrated into Twin Otter aircraft. The relative positions of the CMIGITS IMU, the Imaging Spectrometer, and LiDAR are indicated.

Title: NEON Imaging Spectrometer Geolocation Algorithm Theoretical Basis Document		Date: 11/20/2015
NEON Doc. #: NEON.DOC.001290	Author: T. Kampe, W. Gallery	Revision: B

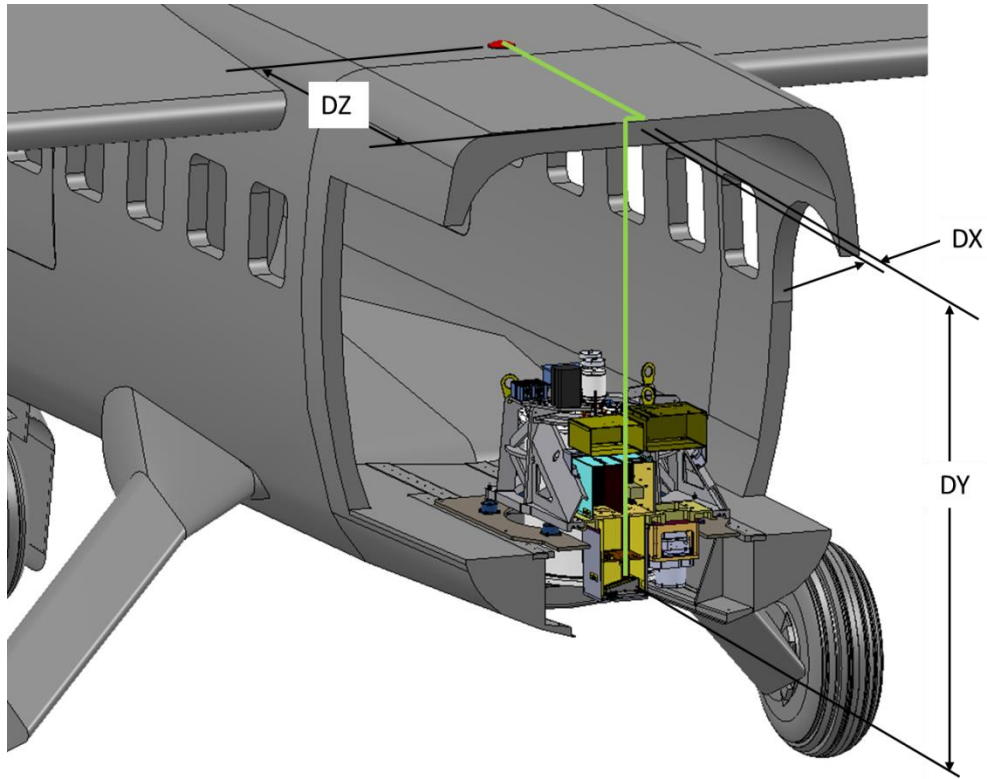


Figure 8. Lever arm calculations for the NISDVU for the configuration flown during May 2012

If the vector between the origin of the INS body frame (b-frame) and the imaging spectrometer entrance pupil is given in the b-frame as a^b , $r_s^m(t)$ can be written as

$$r_s^m(t) = r_{INS}^m(t) + R_b^m(t)a^b \quad 3$$

where

- $r_{INS}^m(t)$ is the vector of the interpolated coordinates of the IMU in the m-frame at time (t);
- $R_b^m(t)$ is the rotation matrix for rotating the b-frame into the m-frame;
- and, a^b is the constant vector between the imaging spectrometer entrance and the center of the IMU b-frame, determined from measurements onboard the aircraft.

In addition to transformations between sensors, the rotations between different sensor reference frames need to be taken into account. The IMU b-frame is not necessarily aligned with the imaging spectrometer sensor reference frame (S-frame), and therefore the constant rotation R_s^b between the two reference frames needs to be established. This is also obtained from measurements on the aircraft. Then the rotation matrix between the S-frame and the m-frame $R_s^m(t)$ can be written for any object point (i) as:

Title: NEON Imaging Spectrometer Geolocation Algorithm Theoretical Basis Document		Date: 11/20/2015
NEON Doc. #: NEON.DOC.001290	Author: T. Kampe, W. Gallery	Revision: B

$$R_s^m(t) = R_b^m(t)R_s^b \quad 4$$

where R_s^b is the rotation between the S-frame and the IMU b-frame determined from measurement.

Substituting Equations (3) and (4) into Equation (1) then yields the final georeferencing formula that can be written as

$$r_i^m = r_{INS}^m(t) + R_b^m(t)(R_s^b r_i^s + a^b) \quad 5$$

The situation with the NEON imaging Spectrometer is further complicated by the fact that the IMU is housed within the LiDAR, and therefore the lever arm from the IMU to the LiDAR scan mirror must also be taken into account when determining the offsets for georeferencing the LiDAR data.

For a more general description of the geolocation algorithm, see Appendix C. Mathematics of Geolocation.

5 ALGORITHM IMPLEMENTATION

5.1 Production Processing Flow

The processing of the raw imaging spectrometer data to the final orthorectified data is achieved in the following steps. These are also represented in the processing flow diagram of Figure 2. A list of the files involved in the processing is included as Appendix B: List of Files.

The imaging spectrometer geolocation algorithm has been implemented in IDL and calls several ENVI functions.

Step 1: Initial processing of the raw data. This step performs the time sync between the imaging spectrometer image frames and navigation data as provided from the LiDAR geolocation processing.

- Inputs: image and sbet files:
 - egm96 geoid file, the desired down track binning factor, a flag to tell it if the raw files are only three bands or full 481-band data, the UTM time zone and file names of the raw image file, the processed radiance file that indicates the starting raw sample and frame, and the sbet navigation file
- Output: ephemeris and attitude files as well as timing files that contain the data needed to ray trace from the pixels on the ground to the imaging spectrometer image plane:
 - Navout_mout : navigation parameter output file containing attitude and ephemeris data for orthorectification.

Step 1b: Conducts a quick ray tracing of the three center pixels and the two edge pixels to find the extent of the corrected images and to gather statistics on the mean down-track and cross-track pixel spacings. Output from a sample Step 1b report file is shown in Table 1.

- Inputs:
 - name of report file to create
 - a mode flag to ray trace only the 5 pixels per line
 - a flag to indicate if ENVI is available
 - the UTM zone, the DEM file to use
 - the names of the navout_mout files created in Step 1
 - the name of the camera file (a unique camera file is generated for each imaging spectrometer)
 - bin factor being used
- Output:
 - Output report

Table 1. Sample Step 1b Report File. The parameters being reported are the minimum and maximum extents of the imaged camera pixels on the ground (in meters) and the down-track pixel spacings (dt_ps) and cross-track pixel spacings (at_ps) in pixel units.

file, xmin, xmax, ymin, ymax, dt_ps, at_ps						
G:\gj0512\20120505\NISDVU20120505t171541	716598.548	721321.618	4326770.690	4330128.230	0.974	3.423
G:\gj0512\20120505\NISDVU20120505t175337	713966.592	718783.890	4326936.518	4331747.816	0.509	1.188
G:\gj0512\20120505\NISDVU20120505t180354	714386.039	719319.931	4328043.058	4332788.129	0.667	1.143
G:\gj0512\20120505\NISDVU20120505t181309	713268.245	718189.197	4327397.653	4332319.707	0.727	1.170
G:\gj0512\20120505\NISDVU20120505t182046	714711.815	719185.100	4327506.004	4331716.742	0.748	1.200
G:\gj0512\20120505\NISDVU20120505t183058	714343.934	718867.336	4328338.821	4332800.522	0.642	1.195
G:\gj0512\20120505\NISDVU20120505t183826	715407.425	719635.856	4328304.897	4332293.735	0.674	1.146
G:\gj0512\20120505\NISDVU20120505t184822	716174.793	717739.346	4327195.717	4333793.142	0.690	1.172
G:\gj0512\20120505\NISDVU20120505t185341	723598.910	725074.293	4330342.646	4337627.588	0.759	1.215
G:\gj0512\20120505\NISDVU20120505t190317	723530.199	724742.111	4330476.697	4337402.323	0.627	1.223
G:\gj0512\20120505\NISDVU20120505t191134	723249.560	724504.693	4329653.243	4337105.527	0.711	1.208
G:\gj0512\20120505\NISDVU20120505t192001	719960.620	727563.370	4332813.361	4334063.034	0.631	1.320
G:\gj0512\20120505\NISDVU20120505t193004	712708.970	720155.165	4329034.319	4334376.288	0.510	0.381
summary values (extreme x,y, min ps) :	712708.970	727563.370	4326770.690	4337627.588	0.509	0.381

Title: NEON Imaging Spectrometer Geolocation Algorithm Theoretical Basis Document		Date: 11/20/2015
NEON Doc. #: NEON.DOC.001290	Author: T. Kampe, W. Gallery	Revision: B

Step 2: This procedure does a full image ray trace of every image pixel to the DEM surface being used, builds the IGM file that contains the x, y, z coordinates of each pixel center.

- Inputs:
 - mode flag to tell program to ray trace all pixels
 - a flag to indicate if ENVI is available
 - the UTM zone
 - the navout_mout files created in Step 1
 - DEM file
 - Camera file
 - Bin factor in use
- Output:
 - IGM file

Step 3: This procedure uses the IGM file created in Step 2 and a user-supplied slope-aspect file (provided through processing of the LiDAR data) to build the OBS file that lists the ten observation geometry parameters:

- 1 Path length
- 2 To-sensor azimuth angle
- 3 To-sensor zenith angle
- 4 To-sun azimuth angle
- 5 To-sun zenith angle
- 6 Phase
- 7 Slope
- 8 Aspect
- 9 Cosine angle
- 10 GPS time

- Inputs:
 - Slope_aspect file
 - IGM files
- Output
 - Builds the OBS file

Step 4: This procedure uses the IGM files to create look up table files for each image strip.

- Inputs:
 - Pixel size, rotation (0 for North up), UTM time zone, and the IGM files
- Output:
 - Builds the GLT look-up tables

Title: NEON Imaging Spectrometer Geolocation Algorithm Theoretical Basis Document		Date: 11/20/2015
NEON Doc. #: NEON.DOC.001290	Author: T. Kampe, W. Gallery	Revision: B

Step 5: This procedure pushes the designated files through the GLT look-up tables to build orthorectified images (i.e., fully orthorectified spectrometer data geo-located with the LiDAR discrete point returns). A sample orthorectified spectrometer image for data acquired over Fruita, Colorado during the May 2012 NISDVU flight deployment is shown in Figure 4.

- Inputs:
 - Names of the ortho files to create
 - Names of the GLT file(s) to use
 - Names of the input file(s)
- Outputs:
 - Builds orthorectify ORT files for one or more input files

6 UNCERTAINTY

The required uncertainty in the Earth location accuracy of the geodesic coordinates computed for individual spatial pixels imaged by the NEON imaging spectrometer is divided into two separate requirements (AD[05]). These are:

AOP-TOR-068 Uncertainty in the knowledge of the position of each spatial pixel on the ground must be less than 0.5 of the imaging spectrometer ground sample distance.

AOP-TOR-069 Uncertainty in the knowledge of the relative position of camera, LiDAR, and spectrometer ground pixels must be less than 0.5 of the imaging spectrometer ground sample distance.

6.1 Analysis of Uncertainty

The accuracy of spectrometer ground pixel locations relate back to the positional and attitude accuracy of the aircraft provided by the onboard GPS and IMU. The initial step in the processing chain is the orthorectification of the discrete LiDAR returns as described in AD[08]. This is a mapping of the discrete LiDAR returns to the Earth surface and generation of a digital elevation model (DEM) from this data onto UTM reference frame. Subsequently, the imaging spectrometer pixels are mapped to the DEM. Therefore, any uncertainty in the Earth location accuracy of geodesic coordinated in the LiDAR-generated DEM will contribute to the uncertainty in imaging spectrometer geolocation estimates. As such, the geolocation error budget has two terms – 1) the geolocation accuracy of the LiDAR processing, and 2) the collocation error between the imaging spectrometer data to the geodesic reference frame defined by the LiDAR DEM.

The uncertainty in the geolocation accuracy of the LiDAR data is determined in the NEON I0 to L1 Discrete Return LiDAR processing (AD[08]). In this document, we are considering the co-registration error of the spectrometer pixels to the LiDAR data. In addition, there are additional factors contributing to the uncertainty in co-registration of these data. These manifest themselves as uncertainties in the

<i>Title:</i> NEON Imaging Spectrometer Geolocation Algorithm Theoretical Basis Document		<i>Date:</i> 11/20/2015
<i>NEON Doc. #:</i> NEON.DOC.001290	<i>Author:</i> T. Kampe, W. Gallery	<i>Revision:</i> B

spectrometer pixel location on the ground with respect to the digital surface model defined by the LiDAR. Contributors to the uncertainty budget include the boresight error uncertainty between the imaging spectrometer and LiDAR, instabilities in the platform integration mount which result from thermal perturbations during flight and vibration environment, and errors in matching up tie-points during the algorithmic optimization process. These uncertainties are quantified in the following section.

6.2 Reported Uncertainty

The vertical accuracy for the ALTM Gemini LiDAR is provided in the LiDAR Delivery Performance Report (AD[10]). The accuracy is a function of altitude. For a nominal survey flight altitude of 1000 m AGL, the reported LiDAR horizontal accuracy is 1/5500 x altitude, or 0.182 m (1 sigma). Other errors contributing to the LiDAR discrete return geolocation uncertainty are provided in AD[08], and these include uncertainty in lever arm measurement, elevation error, and GPS/IMU orientation and positioning errors.

The total error allocated to the LiDAR geolocation error is 0.2 pixels. This provides a floor for geolocation error attainable for the imaging spectrometer but several additional contributors need to be considered to quantify the error in estimating the uncertainty in estimating the location of ground features as imaged by the imaging spectrometer and by returns from the discrete LiDAR (i.e., the co-registration error).

The errors contributing to the co-registration error between the imaging spectrometer and LiDAR are listed in the following table:

Title: NEON Imaging Spectrometer Geolocation Algorithm Theoretical Basis Document		Date: 11/20/2015
NEON Doc. #: NEON.DOC.001290	Author: T. Kampe, W. Gallery	Revision: B

Table 2. Co-registration error budget

Error Source	Budget
Spectrometer boresight error	0.10 pixel
PIM thermal stability	0.10 pixel
PIM mechanical vibration error	0.10 pixel
Error in tie-point optimization	0.15 pixel
Total uncertainty (RSS):	0.23 pixel

Therefore, the uncertainty budget for co-registration between the imaging spectrometer and LiDAR is 0.23 pixel (0.23 m @ 1000 m AGL). The predicted error in geolocation for the imaging spectrometer with respect to the true Earth geodesic coordinates is obtained as the root-sum square of the co-registration uncertainty and the geolocation error:

Table 3. Imaging spectrometer geolocation error

Error Source	Budget
LiDAR geolocation error	0.20 pixel
Spectrometer co-registration error	0.23 pixel
Total uncertainty (RSS):	0.31 pixel

7 VALIDATION AND VERIFICATION

7.1 Algorithm Validation

Validation of the geolocation algorithm consists of two major components: first, the orthorectification of individual pixels with respect to the earth needs to be verified. This is best achieved using accurately geo-referenced ground points distributed across and along a flight line. The error in estimated ground location from the airborne imaging spectrometer data, following application of the geolocation algorithm, can then be estimated.

A series of test flights are planned during the 2014 AOP deployment in Boulder, CO to provide data for data product validation. This involves the accurate measurement of ground control points and the acquisition of imaging spectrometer and LiDAR data at several altitudes over the region. The baseline plan is to measure ground points every 5-meter (or better) along the airport runway used for operations and other nearby buildings to locate corners and edges. These features will then be identified in imagery and optical offsets determined in ground data processing. Absolute horizontal accuracies relative to the ground control points determined using this technique are expected to be better than $\pm 0.05 - 0.08$ meter (Asner *et al.*, 2007).

Secondly, the co-registration of the imaging spectrometer data to the LiDAR intensities needs to be determined to validate that the ground features recorded in both data streams have been co-registered to the specified requirements. The different sampling geometries of the LiDAR and spectrometer

Title: NEON Imaging Spectrometer Geolocation Algorithm Theoretical Basis Document		Date: 11/20/2015
NEON Doc. #: NEON.DOC.001290	Author: T. Kampe, W. Gallery	Revision: B

combined with aircraft motion and local topography produce additional uncertainty in registering the LiDAR and spectrometer data. The data acquired from the test flights described above can be used for co-registration validation. Data acquired at multiple altitudes will provide a range of collection angles and ground sampling sizes. Registering LiDAR data with spectrometer data is expected to be better than 1/3 pixel (Asner *et al.*, 2007). Ultimately, the geolocation accuracy is required to be sub-pixel, our ability to validate this will be limited by the imaging spectrometer spatial sampling. For this reason, a statistical analysis conducted over a number of ground samples may be required to attain the desired validation accuracy.

7.2 Data Product Validation

The algorithm defined in this document produces the orthorectified L1 spectral radiances from raw L0 instrumental data acquired with the imaging spectrometer. The uncertainties in location accuracy of geodesic coordinates computed for individual pixels will be determined experimentally using the calibration procedure described in the previous section. The accuracy is limited by the uncertainty in the aircraft, instrument, and elevation information provided to the algorithm.

8 SCIENTIFIC AND EDUCATIONAL APPLICATIONS

The imaging spectrometer geolocation algorithm provides the intermediate geolocated “at-sensor” radiance product required to produce the orthorectified spectral radiance product. Subsequent processing, including atmospheric correction (RA [04]) are required to produce the L-1 spectral reflectance product as described in RD[05].

It is anticipated that the majority of ecological researchers will utilize the NEON.DOM.SIT.DP1.30006 Spectrometer Surface Directional Reflectance product or higher data products derived from this product in their research. However, it is expected that the geolocated “at-sensor” radiance product will be of interested to some researchers interested in exploratory research or interested in conducting their own atmospheric correction.

9 FUTURE MODIFICATIONS AND PLANS

The imaging spectrometer geolocation algorithm has been fully implemented in research-grade code and operation has been validated using airborne data acquired during the 2012 airborne flight deployments. The current version of the software for this algorithm is written in IDL and requires human interaction at several steps. Future development to be considered may include streamlining, improving, and further automating the code based on operational experience.

Title: NEON Imaging Spectrometer Geolocation Algorithm Theoretical Basis Document		Date: 11/20/2015
NEON Doc. #: NEON.DOC.001290	Author: T. Kampe, W. Gallery	Revision: B

10 BIBLIOGRAPHY

Asner, G. P., D. E. Knapp, T. Kennedy-Bowdoin, M. O. Jones, R. E. Martin, J. Boardman, C. B. Field, 2007. Carnegie Airborne Observatory: In-flight fusion of hyperspectral imaging and waveform light detection and ranging (wLiDAR) for three-dimensional studies of ecosystems, *Jour. Appl. Remote Sens.* (1), 013536 [doi: 10.1117/1.2794018].

Boardman, J. 1999. Precision geocoding of low altitude AVIRIS data: Lessons learned in 1998. R. Green (Ed.), 8th Annual JPL Airborne Earth Science Workshop, Pasadena, CA, JPL **99-17**: 63-68.

El-Sheimy, N., 2009. Georeferencing component of LiDAR systems, in *Topographic Laser Ranging and Scanning*, J. Shan and C. K. Toth, Eds., CRC Press, Boca Raton, FL.

Lichti, D., and J. Skaloud, 2010. Registration and calibration, in *Airborne and Terrestrial Laser Scanning*, G. Vosselman and H-G. Mass, Eds., CRC Press, Boca Raton, FL.

APPENDIX A SCANNING GEOMETRIES OF THE NEON REMOTE SENSING INSTRUMENTS

A.1 Spectrometer Data Acquisition Geometry

The NEON imaging spectrometer (NIS) is a pushbroom spectrometer that provides spectroscopic information at 5 nm continuous samples over the 380 to 2510 nm spectral range with an instantaneous field of view of 1.0 mrad. At a flight altitude of 1500 m, NIS will observe a cross-track swath of 928 m. The IFOV corresponding to a single detector pixel is equivalent to a ground sampling distance (GSD) of 1.5 m at an aircraft altitude of 1500 m (AGL). The concept of a pushbroom imaging spectrometer is illustrated in Figure 8.

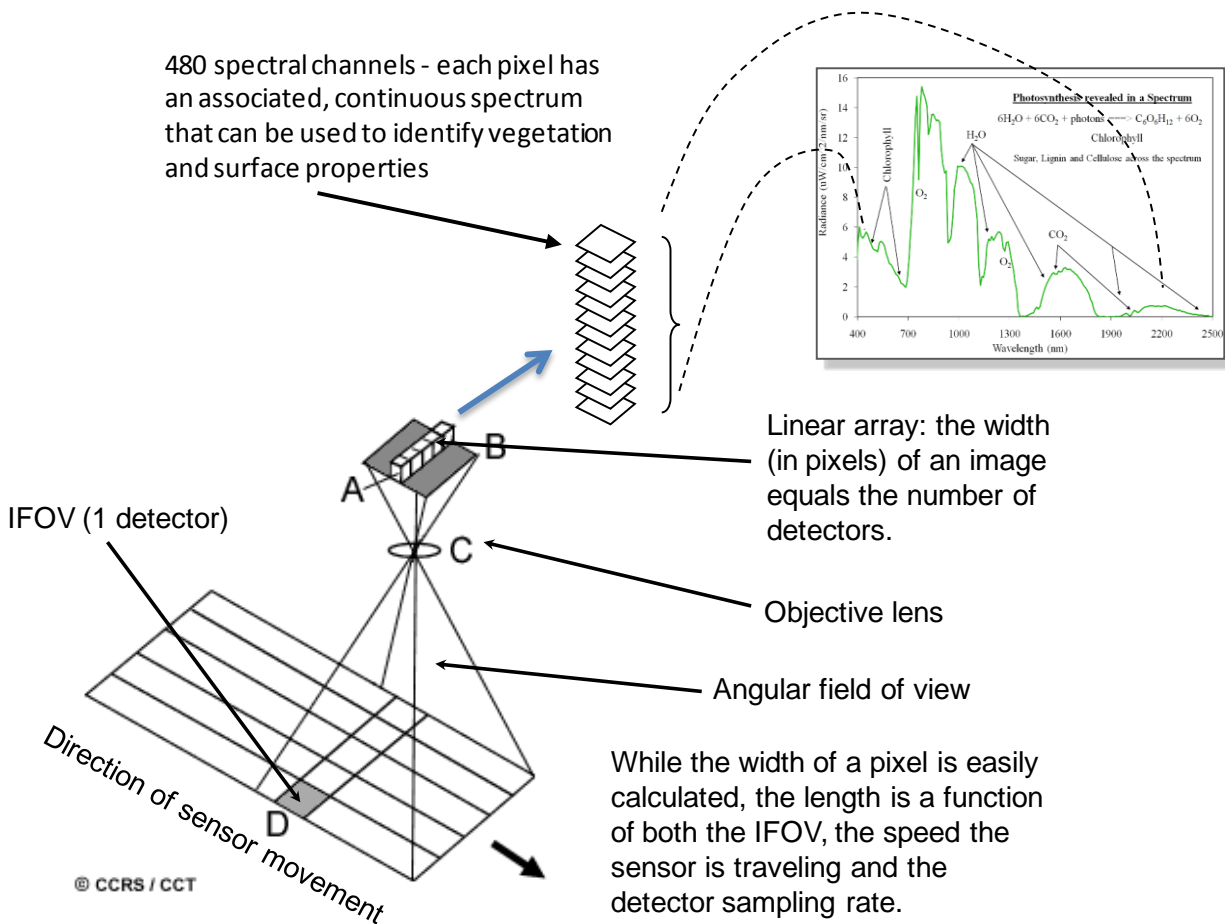


Figure 8. Pushbroom imaging spectrometer concept

The geometry for NIS is shown in Figure 9. The typical flight line is 20 km long and, for a flight altitude of 1500 m, the cross-track swath is 928 m. A single row (line) of 640 cross-track pixels are imaged at a time and data over the full flight line is captured as a result of the forward motion of the aircraft. With an equivalent aircraft ground speed of 50.0 m/sec, 400 seconds or 6.67 minutes are required to scan a single flight line.

Title: NEON Imaging Spectrometer Geolocation Algorithm Theoretical Basis Document		Date: 11/20/2015
NEON Doc. #: NEON.DOC.001290	Author: T. Kampe, W. Gallery	Revision: B

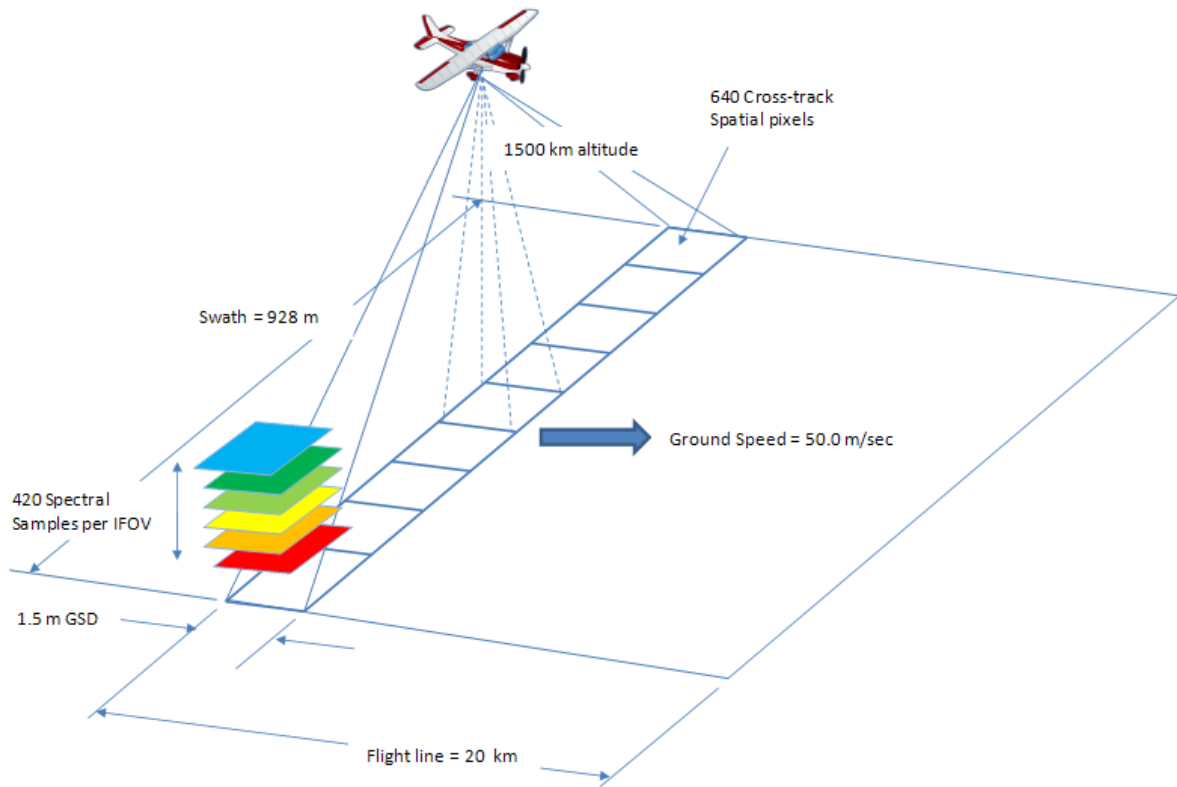


Figure 9. NIS flight geometry

The spectrometer is operated at 100 lines per second, giving a detector integration time of 0.01 sec and resulting in an image smear for a single IFOV_{along-track} equivalent to $(0.01 \text{ sec}) \cdot (50.0 \text{ m/sec})$, or 0.5 m. Therefore the point spread function in the along-track direction $PSF_{\text{along-track}}$ is smeared over 2.0 m (1.5 m + 0.5 m). The along-track ground sample distance is the distance between two consecutive lines on the ground and is equivalent to $(0.01 \text{ sec}) \cdot (50.0 \text{ m/s})$, or 0.5 m. At 100 lines per second, the spectrometer is oversampling the ground in the along-track direction. The cross-track ground sample distance $GSD_{\text{cross-track}}$ is still related to the IFOV, or 1.5 m. Scene radiance is integrated every 0.01 seconds. For each integration period, data in 640 cross-track pixels is recorded. Associated with each cross-track pixel is a column of 480 spectral pixels, each sampling a 5 nm wavelength interval and in total covering the 380 to 2510 nm spectral range. Not all 480 spectra pixels contain valid spectra information, however all 480 are recorded in the raw data. Thus, for any single integration period, data is recorded in $640 \cdot 480$ pixels, or 307,200 pixels total. Each pixel is digitized in a 16-bit word (14 bit dynamic range), resulting in an instantaneous data rate of 4.92×10^6 bits, or 600 Kilobytes. Over a single 20-km flight line, 40,000 along-track lines are acquired, resulting in a total data volume from the NIS instrument of 22.9 GB per flight line. Assuming overlap of 30% between neighboring flight lines, a total of 24 flight lines are required to

Title: NEON Imaging Spectrometer Geolocation Algorithm Theoretical Basis Document		Date: 11/20/2015
NEON Doc. #: NEON.DOC.001290	Author: T. Kampe, W. Gallery	Revision: B

survey a single site. Including one minute of calibration data per flight line (3.4 GB), the data volume per site is estimated as 24 * (22.9 + 3.4 GB), or 635 GB.

A.2 LiDAR Data Acquisition Geometry

The NEON AOP incorporates the Optech ALTM Gemini waveform LiDAR. The specifications for this instrument as compared to key AOP requirements are show in Table A1-1.

Table 4. AOP Waveform Altimeter LiDAR requirements compared to the Optech ALTM Gemini Specification

System Parameter	AOP Requirement	Optech ALTM Gemini Specification
Laser wavelength	1064 nm	1064 nm
Laser pulse width	≤ 10 nsec	10 nsec @ 70 kHz
Laser divergence	≤ 1 mrad	User choice (two selections); 0.3 or 0.8 mrad selectable divergence
Pulse repetition frequency	33 to 100 kHz (>150 kHz goal) selectable	33 – 167 kHz (full waveform up to 70 kHz; sub-samples at higher rates)
Waveform sampling	> 8 bits, 1 nanosecond interval	8 or 12 bits, 1 ns interval
Scan frequency	> 50 Hz (selectable)	0 – 70 Hz
Scan angle	≥ 35 degrees	0 – 50 degrees
Elevation error	< 25 cm (1 σ)	< 5 – 30 cm (1 σ)
Horizontal position error	≤ 0.8 m (1 σ)	1/5,500 x altitude (m AGL) (1 σ)
Aircraft altitude	1000 to 3000 meters AGL (1000 meters to 5000 m above sea level)	150 – 4000 m AGL, nominal*
Ground footprint (nadir)	1 to 3 meters (altitude dependent)	Altitude dependent – function of laser divergence

* Operational eye-safe altitudes

The WALi instrument is a cross-track scanning instrument where a scan mechanism serves to direct the transmitted laser beam across the swath as the aircraft moves forward in the along-track direction. As the aircraft moves forward, as series of cross-track scans are built up until a complete flight track is sampled as shown in Figure A-3. Assuming an aircraft altitude of 1500 m, a scan frequency of 40 Hz, and a total mirror scan angle of 40 degrees, the typical cross-track swath (1092 m) is scanned in 12.5

Title: NEON Imaging Spectrometer Geolocation Algorithm Theoretical Basis Document		Date: 11/20/2015
NEON Doc. #: NEON.DOC.001290	Author: T. Kampe, W. Gallery	Revision: B

milliseconds. The laser pulse repetition frequency is 70 kHz, so a laser pulse is transmitted every 14.3 microseconds. Therefore, there are 875 shots per swath.

The typical flight line is 20 km in length. At a ground speed of 50.0 m/sec, the flight line is sampled in 400.0 sec (~6.7 minutes). Within this time period, a total of 28.0×10^6 shots are sampled (this corresponds to approximately 32,000 cross-track scans). The waveform corresponding to each shot is sampled at 1 nanosecond (ns) intervals. The outgoing pulse is sampled in 40 time bins (1 nsec intervals) and digitized at 12 bits. The return (reflected) pulse is sampled in 440 time bins (also in 1 nsec intervals at 12 bits), resulting in a total of 480 samples per waveform. Therefore, the waveform data volume per flight line is computed as:

$$WALi \text{ Data Volume per flight line} = (n_{shots} * n_{samples} * n_{bits}) / 8 \text{ [bytes]}$$

Where,

$$\begin{aligned} n_{shots} &= \text{number of shots per flight line} = 28.0 \times 10^6 \\ n_{samples} &= \text{number of samples per waveform} = 480 \\ n_{bits} &= \text{number of bits per sample} = 16 \text{ (12 bit stored in 16 bit integers)} \end{aligned}$$

The right-hand term is the conversion factor from bits to bytes (8 bits per byte). Including discrete returns (in LAS 1.2 format) plus some calibration data (assumed to be equivalent to two extra flight lines per site), the total raw data volume for the WALi per flight is then 3.23×10^{10} bytes, or 30.1 GB. This equates to 722.8 GB per site and 2168.3 GB per NEON domain.

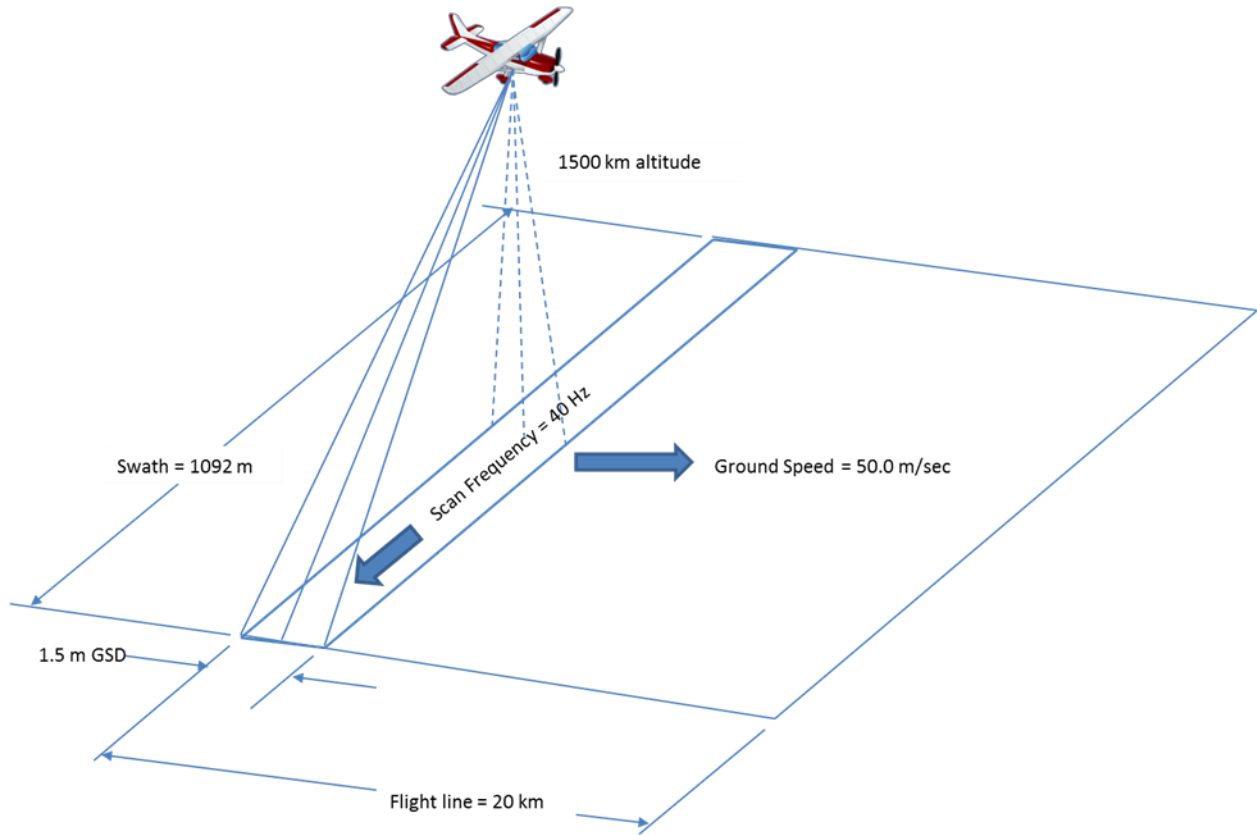


Figure 10. WALi scan geometry

The waveform is obtained by time sampling the laser pulse as it is transmitted from the instrument (outgoing) and as it is returned to the instrument after reflection off the vegetation canopy and ground (incoming or return). The time required for the laser pulse to travel from the aircraft to the ground is

$$t = \text{altitude}/c = 1500 \text{ m}/2.99 \times 10^8 \text{ m/sec} = 5,000 \text{ nsec}$$

Therefore, the round-trip time for a pulse of light from the laser to the ground and back is 10,000 nsec. Assuming 440 time bins are allocated to the return waveform, and each bin is sampled in 1 nanosecond intervals, a continuous range of 66 m can be measured:

$$R = R_2 - R_1 = c * \frac{t_2 - t_1}{2} = \left(\frac{2.998 \times 10^8 \text{ m}}{\text{sec}} \right) * \frac{(440 \times 10^{-9} \text{ sec})}{2} = 66 \text{ m}$$

With an outgoing pulse width of 10 nanoseconds, the range resolution (the separation distance required between two objects to distinguish them as two separate objects) is

$$\Delta R = \frac{c * \tau}{2} = \frac{\left(\frac{2.998 \times 10^8 \text{ m}}{\text{sec}} \right) * (10 \times 10^{-9} \text{ sec})}{2} = 1.5 \text{ m}$$

However, since the return waveform is oversampled at 1 nanosecond bins, using edge detection algorithms surface feature heights can be determined at a range resolution of about 0.15 m. At a pulse

Title: NEON Imaging Spectrometer Geolocation Algorithm Theoretical Basis Document		Date: 11/20/2015
NEON Doc. #: NEON.DOC.001290	Author: T. Kampe, W. Gallery	Revision: B

repetition frequency of 70 kHz, the time between pulses is 14,300 nsec which is larger than the two-way travel time for a single pulse of 10,000 nsec. Thus, only a single laser pulse will be in the atmosphere at any given time and there is no ambiguity as to which pulse is sampled on return to the instrument. In some instances it will be desirable to fly at altitudes other than the nominal 1500 m AGL stated, but the important point is that pulse repetition frequency can be tuned to avoid ambiguity over the range of altitudes that AOP will be operating over.

A.3 Camera Data Acquisition Geometry

The digital camera incorporated into the AOP remote sensing payload is the Applanix DSS 449 camera. Specifications for this camera are summarized in Table 5.

Table 5. Applanix DSS 449 camera specifications

Parameter	Value
Image size	5412 (track) x 7216 (x-track) pixels (39 Mpixels)
Pixel pitch	0.0068 mm
Camera focal length	60.0 mm
Field of view	Along-track: 34 deg; useable 31.5 deg Cross-track: 44 deg; useable 39.3 deg
IFOV	0.00011 radians
Shutter speed	125 - 4000 Hz
Dynamic range	12 bits

The camera is operated in step-stare mode as illustrated in Figure A-4. Here we assume an aircraft altitude of 1500 m, and a ground speed of 50.0 m/sec. Initially, an image is acquired at time t_1 . At a time t_2 , the forward motion of the aircraft causes the camera to image a region some distance D in the along-track direction. Time references are shown at the leading edge of the ground scene in Figure A-4. It is desirable that successive images from the camera capture the ground below in a continuous manner without any gaps. The nominal ground speed of the aircraft is 50.0 m/sec, and for the camera parameters listed in Table A1-2, the along-track image of the detector array is 950 m. Therefore, an image must be acquired every 19.0 sec to obtain gapless imagery. With a camera frame rate of 4000 Hz (i.e., a frame is taken every 0.25 msec), the image smear along track is 0.0125 m. Based on the aircraft altitude and IFOV, the along-track and cross-track GSD at the center of the image (nadir-looking pixel) is 0.17 m.

This situation is somewhat idealized in that it does not account for variation in flight altitude, flight speed, or aircraft orientation which could result in data gaps. To provide margin, we therefore plan to acquire and store frames at shorter time intervals, nominally equal to one-half the time required to traverse the distance equivalent to a full image ($D/2$ in Figure A-4). This is every 9.5 seconds. Thus, every 38,000th frame acquired by the camera is retained as part of the data stream. With a typical flight

line 20 km long (along-track) by 1300 m wide (cross-track), a total of 43 shots/frames are required and the data volume per flight line is calculated as

$$Data\ volume\ per\ flight\ line = (n_{pixels} * n_{bits} * n_{shots}) / 8 \text{ [bytes]}$$

Where:

$$n_{pixels} = \text{total number of pixels} = 3.90 \times 10^7$$

$$n_{bits} = \text{number of bits per sample} = 16 \text{ (12 bits stored in 16 bit integers)}$$

$$n_{shots} = \text{number of shots per flight line}$$

The result is that the camera data volume is 3.1 GB per flight line, or 75.1 GB per site. The details used in the data volume calculation are provided in Table 6.

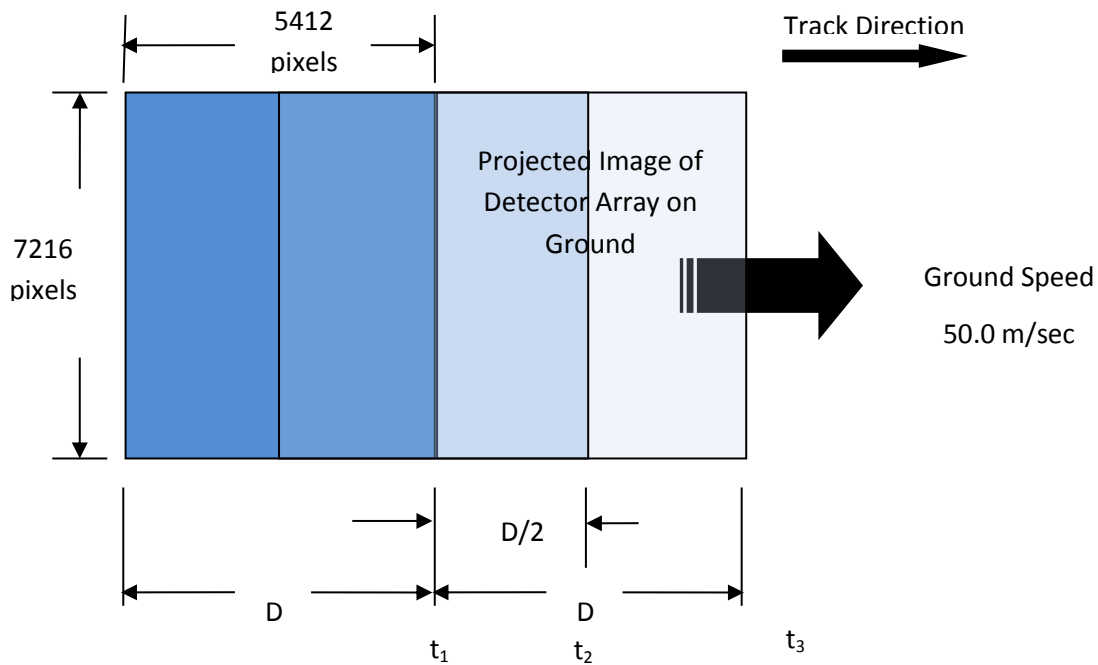


Figure 11. AOP camera scanning approach

Table 6. Typical camera data acquisition parameters

Parameter	Typical Value
Aircraft altitude (AGL)	1500 m
IFOV	0.00011 rad
Geometric GSD_{track} (no smear)	0.17 m
Projected size of detector array on ground	950.0 m (along-track) 1300.0 m (cross-track)

<i>Title:</i> NEON Imaging Spectrometer Geolocation Algorithm Theoretical Basis Document		<i>Date:</i> 11/20/2015
<i>NEON Doc. #:</i> NEON.DOC.001290	<i>Author:</i> T. Kampe, W. Gallery	<i>Revision:</i> B

Parameter	Typical Value
Aircraft ground speed	50.0 m/sec
Length of flight line	20 km
Number of flight lines per site (30% overlap)	24
Time required to distance D/2, D = 950.0 m	9.5 sec
Number of shots per flight line	43
Data volume per flight line	3.1 GB
Data volume per site	75.1 GB

Title: NEON Imaging Spectrometer Geolocation Algorithm Theoretical Basis Document		Date: 11/20/2015
NEON Doc. #: NEON.DOC.001290	Author: T. Kampe, W. Gallery	Revision: B

APPENDIX B LIST OF FILES

Table 7 contains a list of the different file types used in geolocation process.

Table 7. List of input, intermediate and output files

File type	Description
Input	
camera model	contains the camera parameters:
dem	d igital e levation m odel: elevation of the surface on a regular grid
egm	e arth g ravitational m odel:
sap	s lope and a spect: contains the slope and aspect angles of each pixel in the dem
sbt	s moothed b est e stimate of t rajectory: contains the trajectory: location (lat,lon, altitude), attitude (roll, pitch and heading), velocity and acceleration
Intermediate	
eph	ephemeris file: contains
glt	g round l ookup t able: for each raw image pixel, contains the corresponding pixel location in the orthorectified image
igm	contains the x and y locations in UTM of each pixel in a NIS flight line
igm5	as igm, but for only 5 columns in the flight line: the two edges and the 3 central lines
navout_mout	contains x,y,z, roll, pitch, yaw and 3 by 3 attitude rotation matrix for each frame in a flight line
obs	observation file: contains for each raw image pixel: 0: path length 1: sensor azimuth_ 2: sensor zenith 3: sun azimuth 4: sun zenith 5: phase 6: slope 7: aspect 8: cosine of incidence angle 9: gps hour
tim	timing file: contains the gps time for each NIS frame
Output	
rdn_ort	orthorectified radiance
igm_ort	orthorectified igm
obs_ort	orthorectified observation

Title: NEON Imaging Spectrometer Geolocation Algorithm Theoretical Basis Document		Date: 11/20/2015
NEON Doc. #: NEON.DOC.001290	Author: T. Kampe, W. Gallery	Revision: B

APPENDIX C MATHEMATICS OF GEOLOCATION

This appendix describes the coordinate systems used in the geolocation and the methods used to transform the location of an object from one coordinate system to another. It applies both to the spectrometer and to the digital camera.

This discussion is deigned to present an overview of the geolocation process. It does not present enough details to enable the reader to create code to implement the process.

C.1 Vector notation

Consider the right-handed Cartesian coordinate system shown in Figure C-1. The location of the point P is defined by the vector \mathbf{r}_P :

$$\mathbf{r}_P = [x_P, y_P, z_P]$$

eq.
C
-
1

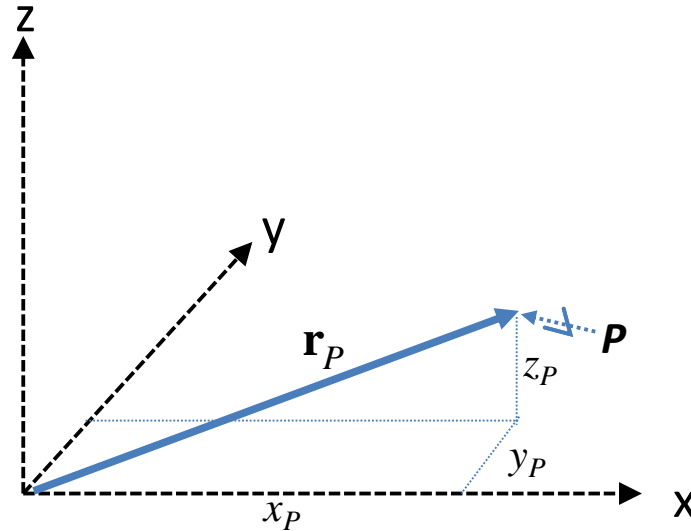


Figure C-1. A right-handed Cartesian coordinate system.

Now consider two coordinate systems, called the b-frame and the s-frame, as shown in Figure C-2. The origin of the s-frame in the b-frame is given by \mathbf{r}_s^b . The location of the point P is given by \mathbf{r}_P^b and \mathbf{r}_P^s in the b- and s-frames respectively. (In this notation, the superscript indicates the reference frame while the subscript indicates the object.)

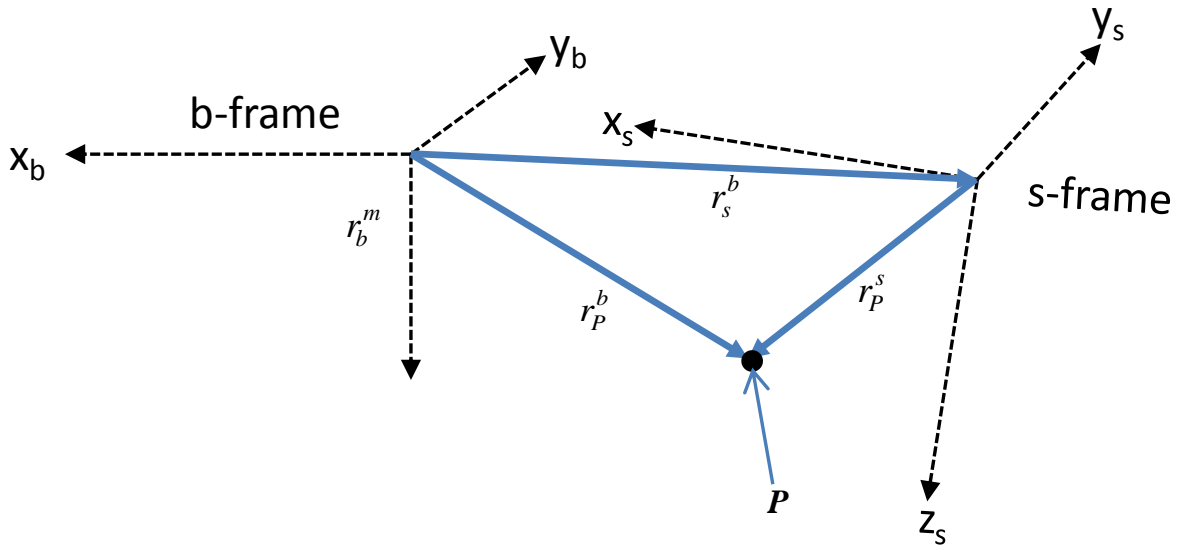


Figure C-2. Relationship between the b-frame and the s-frame.

C.2 Vector rotation: Euler angles

The relative orientation of the two orthogonal coordinate frames can be described in terms of Euler angles. Euler's theorem [Kuipers, 1999] states, for this example that the s-frame can be rotated into the b-frame through a set of successive rotations around the x, y and z-axes. The sequence of the rotations is important: a rotation around the z axis by θ followed by a rotation around the y-axis by ϕ is not the same as a rotation around the y axis by ϕ followed by a rotation around the z axis by θ . In this discussion, we shall standardize on the sequence of rotations around the z, y and x axes in that order. This sequence is known as the Aerospace sequence and involves the application of the yaw (ϕ), pitch (θ) and roll (φ) angles. The Euler angles and their rotations are shown in Figure C-3.

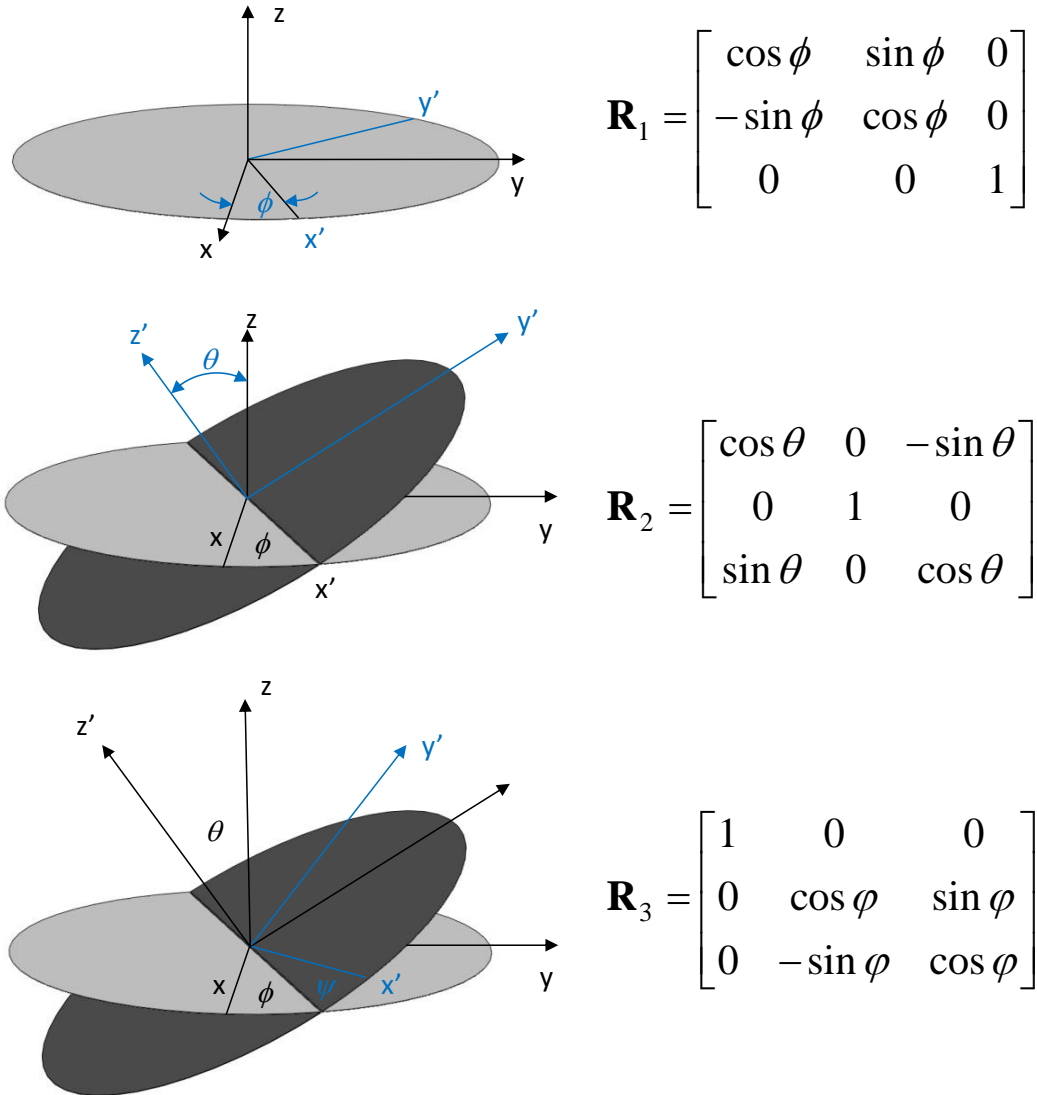


Figure C-3. The three Euler angle (ϕ , θ , ϕ) rotations about the z-axis (yaw), y-axis (pitch) and x-axis (roll.)

Mathematically, let the individual Euler rotations be $\mathbf{R}_1, \mathbf{R}_2, \mathbf{R}_3$ as shown in eq. C-2.

Title: NEON Imaging Spectrometer Geolocation Algorithm Theoretical Basis Document		Date: 11/20/2015
NEON Doc. #: NEON.DOC.001290	Author: T. Kampe, W. Gallery	Revision: B

$$\begin{aligned}
 \mathbf{R}_1 &= \begin{bmatrix} \cos \phi & \sin \phi & 0 \\ -\sin \phi & \cos \phi & 0 \\ 0 & 0 & 1 \end{bmatrix} \\
 \mathbf{R}_2 &= \begin{bmatrix} \cos \theta & 0 & -\sin \theta \\ 0 & 1 & 0 \\ \sin \theta & 0 & \cos \theta \end{bmatrix} \\
 \mathbf{R}_3 &= \begin{bmatrix} 1 & 0 & 0 \\ 0 & \cos \varphi & \sin \varphi \\ 0 & -\sin \varphi & \cos \varphi \end{bmatrix}
 \end{aligned}
 \tag{eq. C-2}$$

Applying these three rotations sequentially leads to the equivalent rotation \mathbf{R} given in eq. C-3.

$$\begin{aligned}
 \mathbf{R} &= \mathbf{R}_3 \mathbf{R}_2 \mathbf{R}_1 \\
 \mathbf{R} &= \begin{bmatrix} \cos \varphi \cos \theta & \sin \varphi \cos \theta & -\sin \theta \\ \left(\begin{matrix} \cos \phi \sin \theta \sin \varphi \\ -\sin \phi \cos \varphi \end{matrix} \right) \left(\begin{matrix} \sin \phi \sin \theta \sin \varphi \\ +\cos \phi \cos \varphi \end{matrix} \right) & \cos \theta \sin \varphi \\ \left(\begin{matrix} \cos \phi \sin \theta \cos \varphi \\ +\sin \phi \sin \varphi \end{matrix} \right) \left(\begin{matrix} \sin \phi \sin \theta \cos \varphi \\ -\cos \phi \sin \varphi \end{matrix} \right) & \cos \theta \cos \varphi \end{bmatrix}
 \end{aligned}
 \tag{eq. C-3}$$

Referring back to Figure C-3, we can write:

$$\mathbf{r}_p^b = \mathbf{r}_s^b + \mathbf{R}_s^b \mathbf{r}_p^s
 \tag{eq. C-4}$$

where \mathbf{R}_s^b is the rotation matrix from the s-frame to the b-frame.

C.3 AOP Coordinate systems

The NEON AOP involves three coordinate systems:

1. m-frame: an earth-centered coordinate system.
2. b-frame: a coordinate frame fixed in the aircraft, and
3. s-frame: a coordinate frame fixed in the camera

The m-frame is an earth-fixed map projection, e.g., UTM Zone11N WGS84 or latitude/longitude [Snyder, 1987]. Typically the m-frame will have its y-axis pointing toward geodetic north, its x-axis pointed east and its z-axis pointing vertically upwards opposite the direction of local gravity to complete a right-handed system.

Title: NEON Imaging Spectrometer Geolocation Algorithm Theoretical Basis Document		Date: 11/20/2015
NEON Doc. #: NEON.DOC.001290	Author: T. Kampe, W. Gallery	Revision: B

The b-frame (body-frame) is fixed in the aircraft, specifically with respect to the position and orientation system (POS). The POS consists of the global positioning **satellite** (GPS) system and the inertial positioning unit (IMU) which together provides the location and orientation of the b-frame as a function of time. The origin of the b-frame is located in the IMU and it is oriented approximately with the x-axis pointing toward the nose of the aircraft, the y-axis pointing along the right wing and the z axis pointing down

The s-frame (sensor frame) is fixed in the sensor (spectrometer or camera.) The z-axis of the s-frame corresponds to the sensor boresight. The sensor and the IMU are rigidly fixed to the payload integration mount (PIM) so that the relationship between the s-frame and the b-frame (offset and orientation) is time independent but can change when the instruments are re-installed on the PIM.

Figure C-4 sketches the relationship among the three frames. All three frames are right-handed systems. In this figure, the vector \mathbf{r}_u^v represents the location of the origin of the *u-frame* with respect to the *v-frame*. Note that the offset between the b- and the s-frames is greatly exaggerated for clarity: the separation is less than a meter.

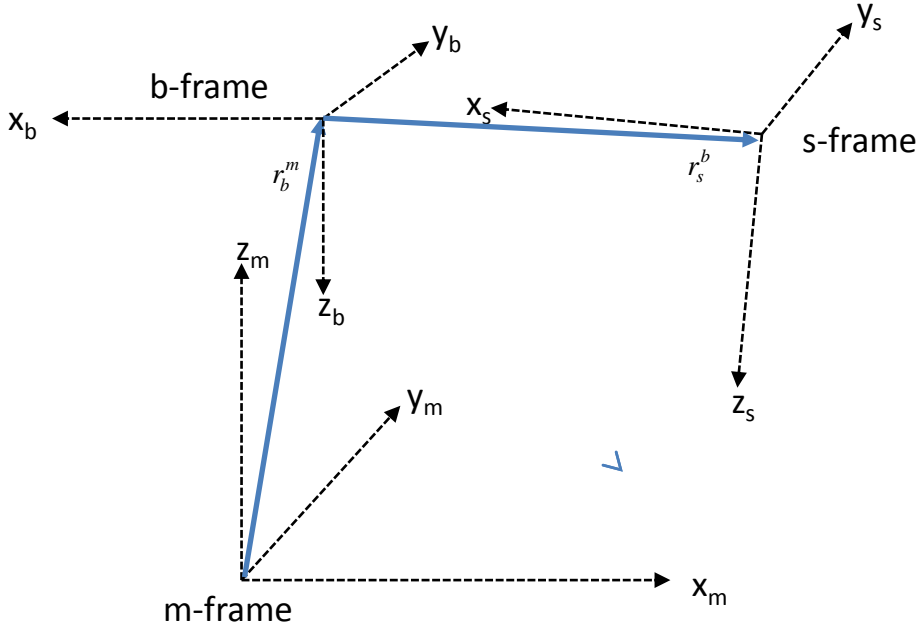


Figure C-4. Sketch showing the m-frame, b-frame and s-frame.

The offset between the origins of the b-frame and the s-frame is called the “lever arm” and is indicated by the vector $\mathbf{r}_s^b = (x_L, y_L, z_L)$ as shown in Figure C-5.

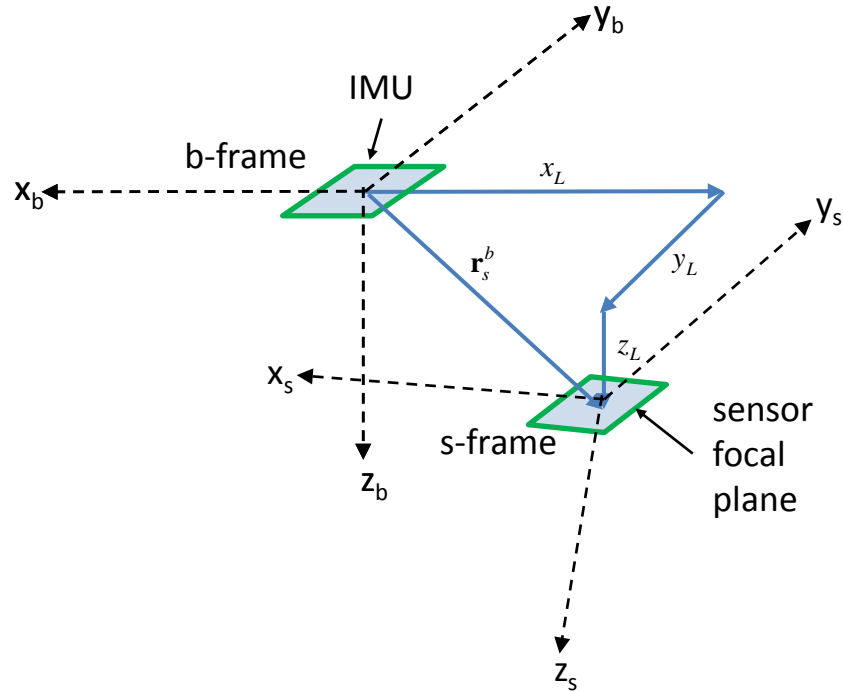


Figure C-5. Sketch showing the b-frame, the s-frame and the lever arm \mathbf{r}_s^b between the IMU and the sensor focal plane.

The location of the b-frame relative to the m-frame is provided by the POS. The data from the POS is processed into a smoothed best estimate of trajectory (sbet) file. This file contains the position (latitude, longitude and altitude) and attitude (roll, pitch and heading.) of the b-frame with respect to the m-frame as a function of time. The time-dependent values of \mathbf{r}_b^m and \mathbf{R}_b^m are obtained from this file. Table C-1 lists all the variables given in the sbet file. In this list, the location is given by the latitude, longitude and elevation while rotations are given by the roll, pitch, heading and wander.

Table C-1 Variables reported in the sbet file

#	Variable	Description
1	time	GPS time as seconds of week since Sunday at 00:00
2	latitude	latitude, in radians
3	longitude	longitude, in radians
4	altitude	altitude in meters referenced to the WGS84 ellipsoid
5	x velocity	velocity in the x direction, in m/s
6	y velocity	velocity in the y direction, in m/s
7	z velocity	velocity in the z direction, in m/s
8	bank	bank (roll), angle in radians

Title: NEON Imaging Spectrometer Geolocation Algorithm Theoretical Basis Document		Date: 11/20/2015
NEON Doc. #: NEON.DOC.001290	Author: T. Kampe, W. Gallery	Revision: B

#	Variable	Description
9	elevation	elevation (pitch) angle, in radians
10	heading	heading (yaw) angle, $-\pi/2$ to $\pi/2$, in radians
11	wander	wander angle, in radians
12	x acceleration	acceleration in the x direction, in m/s ²
13	y acceleration	acceleration in the y direction, in m/s ²
14	z acceleration	acceleration in the z direction, in m/s ²
15	x angular rate	rotation rate around the x axis, in rad/s “
16	y angular rate	rotation rate around the y axis, in rad/s “
17	z angular rate	rotation rate around the z axis, in rad/s “

Notes:

1. x, y, and z refer to the axes of the b-frame.
2. The wander angle must be subtracted from the heading to get heading relative to true North [Jekeli, 2001]

C.4 Camera model

A camera model is a function that describes the LOS of each pixel of the sensor in the b-frame¹. The LOS of a pixel can be described in the s-frame as a unit vector $\mathbf{e}_{i,j}^s$ from the center of the pixel i,j passing through the focal point f :

$$\mathbf{e}_{i,j}^s = (u_{i,j}, v_{i,j}, w_{i,j})$$

eq.
C
-
5

where:

- i, j are the indices of the pixel, and
- $u_{i,j}, v_{i,j}, w_{i,j}$ are the direction cosines of the LOS from the pixel i, j through the focal point f .

¹ Normally, a camera model is referenced to the s-frame. However, here we reference the camera model to the b-frame by including the effects of the lever-arm and alignment offset between the s- and the b-frames.

Figure C-6 sketches the LOS of a pixel for both the spectrometer and the digital camera. Note that the spectrometer is a pushbroom sensor with 598 pixels in the cross-track direction while the digital camera is an imager with an 8984 by 6732 pixel detector, as shown. (Note: for the spectrometer, j is always 0, using zero-based indices).

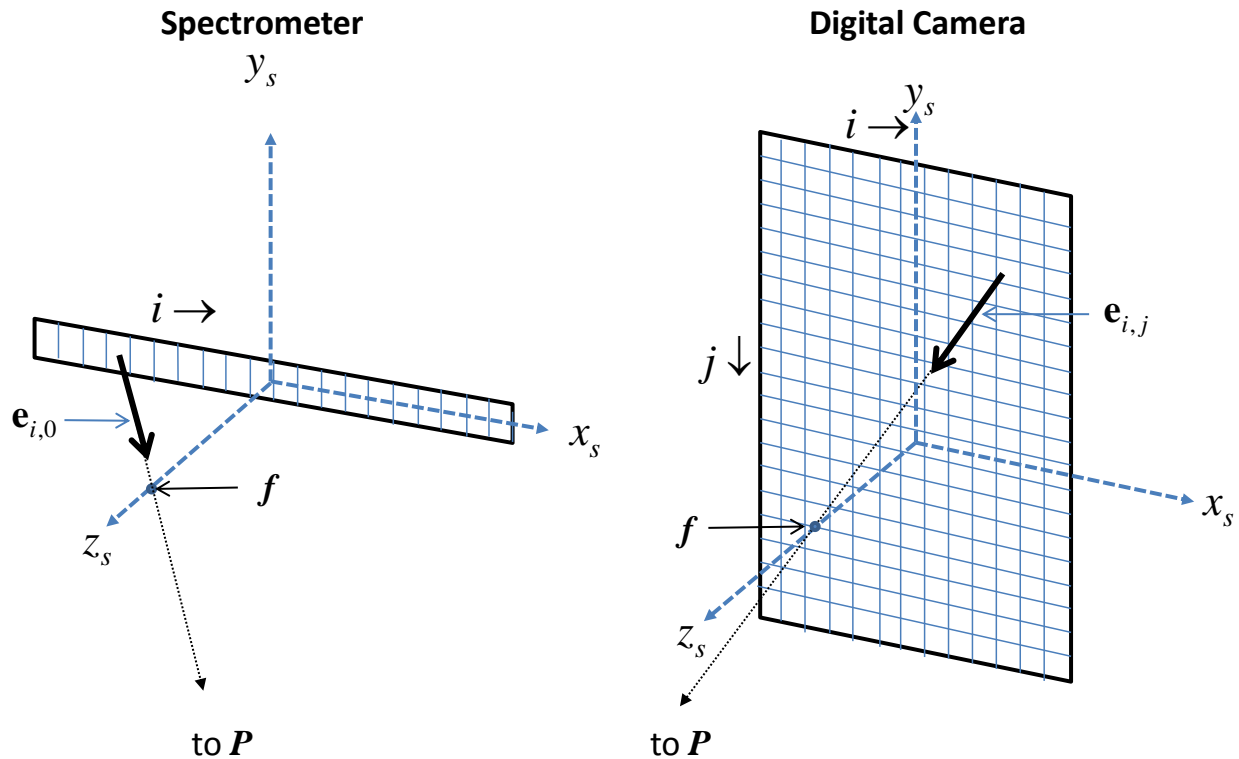


Figure C-6. Sketch showing the LOS of a detector pixel for both the spectrometer and the digital camera. x_s, y_s, z_s are the axes of the s-frame, $e_{i,j}$ is the unit vector for the pixel i,j and f is the focal point.

The camera model includes the effects of both geometric optics and optical distortion. The model can be expressed either as a mathematical function of a set of parameters or as an array of values, one for each pixel. As a function, the camera model can be written as:

$$\mathbf{e}_{i,j}^s = \mathbf{M}(i, j, C_{1,2,3,\dots,N})$$

eq.
C
-
6

where $C_{1,2,3,\dots,N}$ are the camera model parameters. The LOS can be expressed in the b-frame by:

$$\mathbf{e}_{i,j}^b = \mathbf{r}_s^b + \mathbf{R}_s^b \mathbf{e}_{i,j}^s$$

eq.
C
-

<i>Title:</i> NEON Imaging Spectrometer Geolocation Algorithm Theoretical Basis Document		<i>Date:</i> 11/20/2015
<i>NEON Doc. #:</i> NEON.DOC.001290	<i>Author:</i> T. Kampe, W. Gallery	<i>Revision:</i> B

The values of the camera model are obtained by a fitting procedure described elsewhere (see the section- “Calculating the camera parameters”.)

C.5 Geolocation and orthorectification

Orthorectification is the process of re-projecting an image from the s-frame to the m-frame. Geolocation is the process of determining where each sensor pixel LOS in the s-frame intersects the ground, as sketched in Figure C-7. The “ground” is defined by a digital elevation model (DEM) which is the elevation of the surface above the x-y plane of the m-frame². The DEM is defined on a regular grid in the m-frame, ideally at a spatial resolution equal or greater than the resolution of the image.

² The surface can either be the bare earth with all vegetation (e.g., trees) and structures (e.g., buildings) removed—a digital terrain model (DTM) — or the earth including those objects – a digital surface model (DSM). The difference is important but will be ignored for the current discussion.

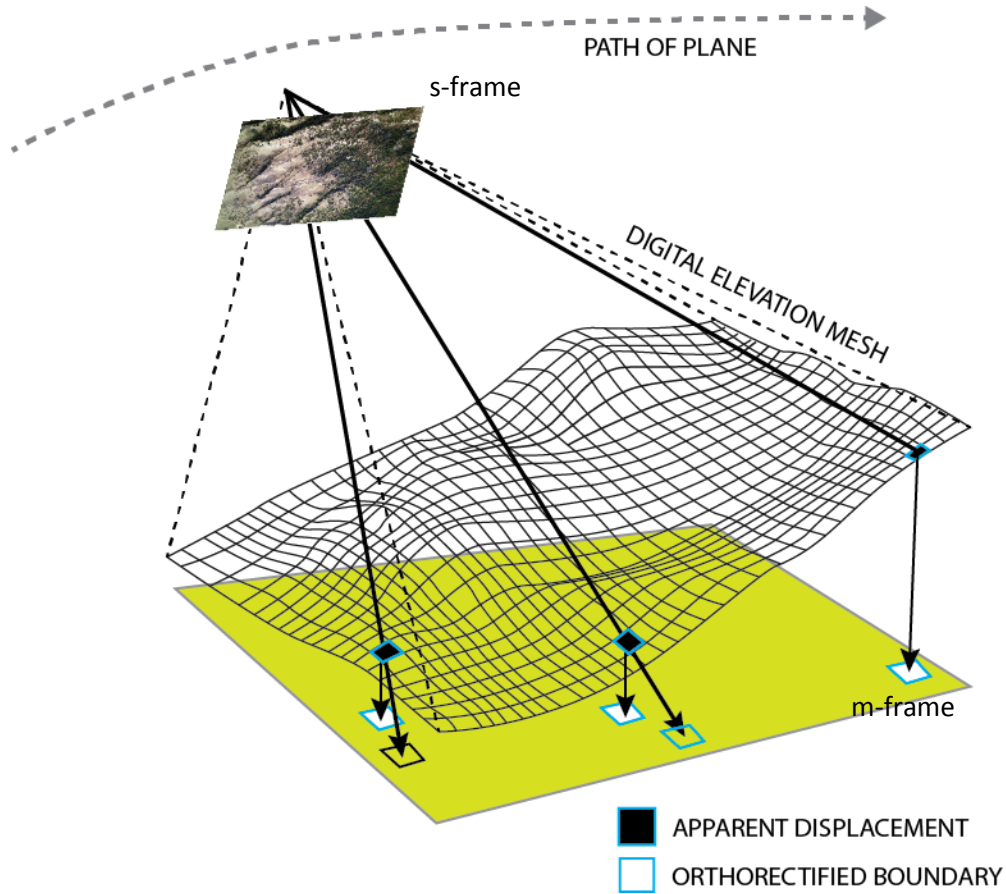


Figure C-7. Sketch of the image observation.

The first step in orthorectification is to define a regular grid in the m-frame that includes the entire field-of-view of the sensor image. The outline of this grid is determined by tracing a ray from each of the edge pixels of the sensor image down to the ground (this procedure will be described later.) The image grid in the m-frame is then the smallest regular grid that encloses this boundary. Note that some pixels in this grid lie outside of the sensor FOV and will not be populated.

Once the image grid is defined, there are two options for populating the pixels: “shooting down” and “shooting up”. In shooting down, each sensor LOS $e_{i,j}^s$ is traced down to where it intersects the ground at P . The sensor pixel value is used to populate the image pixel corresponding to the point P . In shooting up, each image pixel is traced up from P to the corresponding pixel in the sensor frame and the value there is used to populate the image pixel.

C.5.1 Shooting down

In Figure C-8, let the point P be the point on the ground (the DEM) intersected by the LOS $e_{i,j}^s$ from the sensor. The projection of P down to the m-frame intersects an image grid cell k,l . The intent is to determine the location of P . There is no analytic solution to this problem, rather an iterative solution must be employed that extends the ray from $e_{i,j}^s$ down in steps until P is encountered. The details of this procedure will not be presented here. However, the LOS of the sensor pixel i,j in the m-frame is given by Figure C-8.

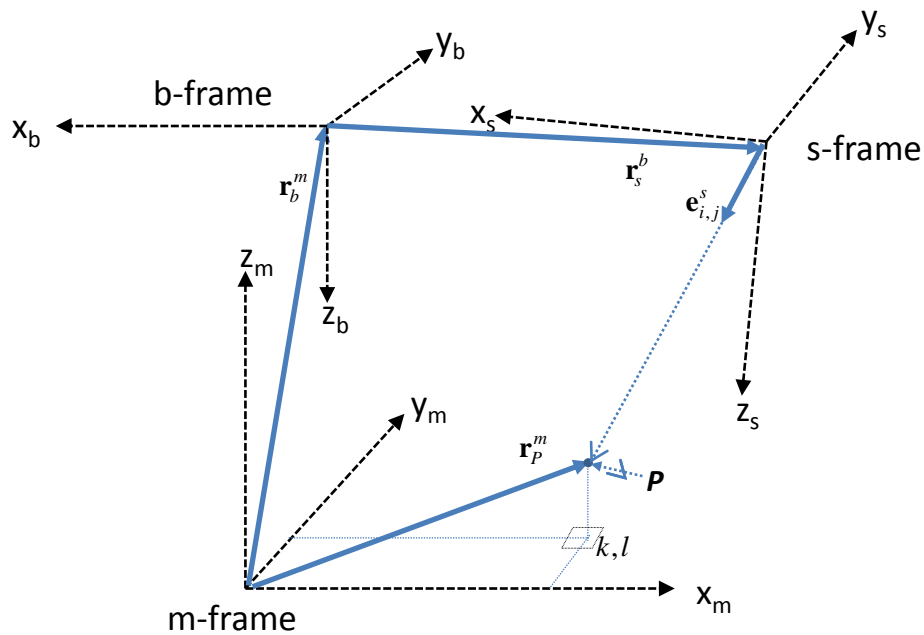


Figure C-8. The location of the point P relative to the m-frame, the b-frame and the s-frame.

$$e_{i,j}^m = r_b^m + R_b^m (r_s^b + R_s^b e_{i,j}^s)$$

eq.
C
-
8

C.5.2 Shooting up

Again in Figure C-8, consider the image grid cell k,l and its associated point P at the surface. We can trace a ray from P through to the focal point of the sensor to where it intersects the sensor x-y plane at pixel i,j as shown in Figure C-9. This process is repeated for each pixel k,l in the image grid. Image grid points that fall outside of the sensor FOV are populated with a value representing “missing data”.

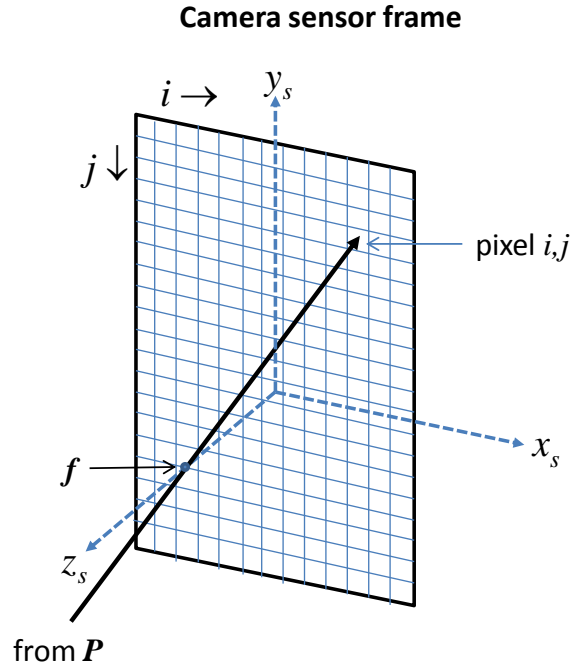


Figure C-9. Sketch showing the LOS from the point P through the focal point f to where it intersects the camera sensor frame at pixel i,j .

Mathematically, the process is:

$$\mathbf{r}_f^m = \mathbf{r}_b^m + \mathbf{R}_b^m (\mathbf{r}_s^b + \mathbf{R}_s^b \mathbf{r}_f^s)$$

eq.
C
-
9

$$\mathbf{e}_{k,l}^b = \mathbf{R}_m^b \left[\frac{(\mathbf{r}_f^m - \mathbf{r}_{k,l}^m)}{|\mathbf{r}_f^m - \mathbf{r}_{k,l}^m|} \right]$$

eq.
C
-
1
0

$$(i, j) = \mathbf{M}^{-1} (\mathbf{e}_{k,l}^b, C_{1,2,3,\dots,N})$$

eq.
C
-
1
1

where:

\mathbf{r}_f^m is location of the sensor focal point in the m-frame,

$\mathbf{r}_{k,l}^m$ is the location of the point on the ground above the pixel k,l in the m-frame, and

Title: NEON Imaging Spectrometer Geolocation Algorithm Theoretical Basis Document		Date: 11/20/2015
NEON Doc. #: NEON.DOC.001290	Author: T. Kampe, W. Gallery	Revision: B

\mathbf{M}^{-1} is the inverse of the camera model, i.e., given the LOS $\mathbf{e}_{k,l}^b$, it returns the corresponding pixel indices i,j

C.5.3 Shooting down vs shooting up: tradeoffs

The choice of which approach to use is governed by the following tradeoffs:

1. Shoot up is computationally much more efficient than shoot down: there is an analytical solution and no iterative algorithm is needed.
2. Shoot down better preserves the fidelity to the original data: each record (spectrum or image pixel) is individually honored and proper located.

The digital camera geolocation algorithm uses the shoot up approach while the spectrometer geolocation algorithm uses the shoot up approach.

C.6 Bibliography

Jekeli, C. (2001), *Inertial navigation systems with geodetic applications*, Walter de Gruyter, Berlin ; New York.

Kuipers, J. B. (1999), *Quaternions and rotation sequences: a primer with applications to orbits, aerospace, and virtual reality*, Princeton University Press, Princeton, N.J.

Snyder, J. P. (1987), *Map projections—A working manual*, 1395, USGPO.